WORMHOLE CHARACTERIZATION USING NUCLEAR MAGNETIC RESONANCE (NMR)

BY

Yaser Khaled Al-Duailej

A Thesis Presented to the
DEANSHIP OF GRADUATE STUDIES

KING FAHD UNIVERSITY OF PETROLEUM & MINERALS

DHAHRAN, SAUDI ARABIA

In Partial Fulfillment of the
Requirements for the Degree of

MASTER OF SCIENCE

In

PETROLEUM ENGINEERING

March 2014

KING FAHD UNIVERSITY OF PETROLEUM & MINERALS

DHAHRAN- 31261, SAUDI ARABIA

DEANSHIP OF GRADUATE STUDIES

This thesis, written by **Yaser Khaled Al-Duailej** under the direction his thesis advisor and approved by his thesis committee, has been presented and accepted by the Dean of Graduate Studies, in partial fulfillment of the requirements for the degree of **MASTER OF SCIENCE IN PETROLEUM ENGINEERING.**

M. Mahmud

Dr. Mohamed A. Mahmoud
(Advisor)

Dr. Abdullah S. Al-Sultan
Department Chairman

Dr. Sidqi A. Abu-Khamsin
(Member)

Dr. Salam A. Zummo
Dean of Graduate Studies

Dr. Mohammad H. Al-Khaldi
(Member)

٢٥/٥/١٤

Date

عمادة الدراسات العليا
DEANSHIP OF GRADUATE STUDIES

Dedication

I dedicate this work to my inspiring parents, to my loving wife, and to my youthful son.

ACKNOWLEDGMENTS

First of all, thanks to Allah, for his guidance and the strength he's given me to complete this work. I would like also to sincerely thank:

- Dr. Mohammed Mahmoud for his guidance and support.
- Dr. Mohammed Al-Khaldi for his supervision.
- Dr. Sidqi Abu-Khamsin, for his valuable efforts and advice.
- Dr. Abdullah Al-Sultan for his support since the inception of the thesis idea.
- Dr. Hyung Kwak for his efforts in the NMR analysis.
- Mr. Ibrahim Al-Yami for his efforts in the coreflooding.
- Dr. Sinan Caliskan and Mr. Abdullah Shebatalhamd for their efforts in the CT scan analysis.
- Mr. James Funk and Dr. Ahmed-Al Harbi for their support in the micro-CT analysis and visualization.
- Mr. Bader Al-Harbi for his support throughout the work of the thesis.
- Saudi Aramco for their support with the equipment and materials.

TABLE OF CONTENTS

LIST OF TABLES

LIST OF FIGURES

LIST OF ABBREVIATIONS

NMR	:	Nuclear Magnetic Resonance
CT scan	:	Computed Tomography scan
pH	:	A measure of the acidity or basicity of an aqueous solution
PV	:	Pore Volume
PV_{BT}	:	Pore Volume to Breakthrough
HT	:	High Temperature
md	:	Millidarcy (permeability unit)
bp	:	Back-Pressure
H^1	:	Proton
T_1 and **T_2**	:	Relaxation Times in NMR
CPMG	:	Carr-Purcell-Meiboom-Gill sequence method for NMR
cm^3/min	:	Cubic Centimeter per Minute (Flow Unit)

ABSTRACT

Full Name : Yaser Khaled Al-Duailej

Thesis Title : WORMHOLE CHARACTERIZATION USING NUCLEAR MAGNETIC RESONANCE (NMR)

Major Field : Petroleum Engineering

Date of Degree : March 2014

Acidizing is a common practice aspired to regain initial skin factor or even reduce it further. Acids tend to create conductive channels, usually referred to as wormholes, through carbonate formations connecting the reservoir to the wellbore and bypassing damaged zones. Optimum wormholes are formed when certain conditions are met, such as optimum acid concentration and injection rate. In order to thoroughly comprehend wormholes, several characterization techniques should be performed.

Computerized tomography (CT) scan and differential pressure data are two common practices to characterize wormholing in laboratories using core plug samples. Differential pressure data and CT scan can verify acid breakthrough occurrence, and qualitatively suggest the size and path of a wormhole. In this study, nuclear magnetic resonance (NMR) was introduced as a new characterization tool for wormholes. In addition, this study shows a comparison between four acid systems at different injection rates, pH values and lithologies, namely reservoir core plug samples and Indiana limestone samples.

The pore size distribution, provided by NMR technique, can indicate the new wormhole porosity by comparing two stages of pre- and post-acidizing. The different acid systems generated unique wormholes, which was used to validate the NMR technique.

Hydrochloric acid (HCl), emulsified acid, and two chelating agents were used to create wormholes using core plug samples from two carbonate formations. NMR was able to accurately analyze, in terms of pore size distribution, different characteristics of the wormholing process of an acid and was consistent with and complementing the CT scan analysis. Furthermore, NMR was able to indicate the changes in interconnectivity between different pore systems and detect the materialization of formation damage. Moreover, emulsified acid has shown the best performance using different injection rates and core plug samples. The performance of Chelating Agent I was dependent on injection rate, pH value and lithology. Chelating Agent II showed dependence on pH value and lithology, whereas HCl showed dependence on lithology.

ملخص الرسالة

الاسم الكامل: ياسر بن خالد الدعيلج

عنوان الرسالة: توصيف الثقوب باستخدام الرنين النووي المغناطيسي

التخصص: هندسة بترولية

تاريخ الدرجة العلمية: مارس 2014

تحفيز الانتاج باستخدام تقنية ضخ الأحماض هو ممارسة شائعة تطمح لاستعادة أو زيادة النفاذية للطبقة الصخرية. الأحماض عادة ما تكوّن قنوات موصلة، يشار اليها باسم الثقوب، خلال طبقات صخور الكربونات لربط مكمن النفط أو الغاز بالبئر المنتجة و تجاوز المناطق التالفة حول البئر. تتشكل الثقوب المثلى عندما يتم استيفاء شروط معينة مثل التركيز الأمثل للحمض و معدل الحقن. لكي تُفهم هذه الثقوب بشكل دقيق، لابد من تنفيذ عدة تقنيات للتوصيف.

التصوير المقطعي المحوسب و فرق قيم الضغط يعتبران من الطرق الشائعة لتوصيف الثقوب في المختبرات باستخدام عينات الصخور الأسطوانية. يمكن باستخدام البيانات المستقاة من اختباريْ فرق الضغط و الاشعة المقطعية للتحقق من حدوث اختراق كامل للحمض، والتنويه بشكل نوعي عن حجم و مسار الثقب. في هذه الدراسة ، تم إدراج الرنين النووي المغناطيسي كأداة جديدة لتوصيف الثقوب. بالإضافة إلى ذلك، تقارن هذه الدراسة بين الأحماض الأربعة باستخدام معدلات حقن مختلفة، أرقام هيدروجينية متغيرة و عينات صخرية متشابهة الخواص من مكمن نفط محلي و من صخور إنديانا الكلسية.

البيانات المستفادة من توزيع أحجام المسامات، و التي تقدمها تقنية الرنين النووي المغناطيسي ، يمكن أن تشير إلى الثقوب المسامية الجديدة، التي تكونت بسبب إذابة الحمض لجزء من العينة الصخرية، من خلال مقارنة العينة قبل و بعد حقن الحمض من خلالها. ويمكن للأحماض المختلفة تكوين ثقوب فريدة بحسب نوعها، مما ساعد في التحقق من صحة تقنية الرنين المغناطيسي النووي كأداة لتوصيف الثقوب. في هذه الدراسة، تم استخدام حمض الهيدروكلوريك، وحمض مستحلب مكون من حمض الهيدروكلوريك المغلف بالديزل، و نوعين من مواد التمخلب لتكوين الثقوب باستخدام عينات الصخور الأسطوانية من طبقات الكربونات. تقنية الرنين النووي المغناطيسي كانت قادرة على تقديم تحليل دقيق، من حيث توزيع أحجام المسامات، و الخصائص المختلفة لعملية التثقيب باستخدام الأحماض. و كانت التحاليل متوافقة مع و مكملة لتحاليل الأشعة المقطعية. علاوة على ذلك، كانت تقنية الرنين المغناطيسي النووي قادرة على تبيين التغيرات المحدثة في الترابط بين الأنظمة المختلفة للمسامات واكتشاف حدوث التلف داخل العينة. بالنسبة للأحماض المستخدمة في هذه الدراسة، فقد أظهر الحمض المستحلب أفضل النتائج

باستخدام مختلف معدلات الحقن وعينات **الصخور**. أما مادة التمخلب الأولى فقد اعتمد تأثيرها على معدل الحقن، وقيمة الرقم الهيدروجيني والخصائص الصخرية للعينات المستخدمة. تأثير مادة التمخلب الثانية اعتمد على قيمة الرقم الهيدروجيني والخصائص الصخرية، في حين أظهرت نتائج حمض الهيدروكلوريك اعتماداً واضحاً على الخصائص الصخرية.

1 CHAPTER 1

INTRODUCTION

The purpose of performing well stimulation is to improve the formation permeability or bypass the damaged zones. Fracturing and matrix acidizing are the two key techniques of well stimulations. Acid stimulation is employed to facilitate the flow in the near wellbore area, while fracture stimulation resolves flow impediments of the reservoir in a far larger area. High percentage of flow constraints are primarily a result of formation damage around the wellbore. This formation damage is triggered by different factors such as drilling fluid filtrate invasion, mud cake creation and scale deposition. Acidizing sandstone formations takes place by dissolving clays and quartz to clear the way for flowing fluids. In carbonates, acid stimulation generates channels that evade the damaged zones to reach the unharmed part of the reservoir. The complication of applying acid stimulation is a combination of suitable designs, reservoir conditions and lithology. The complexity increases with elevated temperatures, and deeper and tighter reservoirs.

Acids ideally react with carbonate formations to form conductive channels connecting the wellbore to the reservoir. These conductive channels are often referred to as wormholes, which are the result of several chemical and physical processes, including acid diffusion, reaction kinetics and dynamics of fluid flow in porous media (Buijse 1997). The chemical reactions of stimulation fluids with the rock are different from one acid/fluid type to another. The reservoir conditions tremendously influence the reaction products and the

performance of the acid stimulation operation. Effective wormholes are characterized by the breakthrough of a core plug sample (in the laboratory), or by extending to a certain distance around the wellbore (in the field). Stimulation fluids can reach deeper into the formation and minimize the face dissolution phenomena when favorable conditions are met. The key elements that govern the creation of wormholes are: 1) acid strength and concentration, 2) rock composition, 3) injection rate, and 4) temperature and pressure. For example, the reaction rate of stimulation fluid with calcium carbonate has to be slow to create conductive and deep wormholes. The reaction between strong acids, e.g. hydrochloric acid (HCl), and calcite (calcium carbonate) is extremely rapid and vigorous, while weak acids, such as organic acids or chelating agents, react rather gradually with calcite. Therefore, slow reacting acids are more likely to create wormholes than strong acids. At high temperatures, the reaction rate of any given acid and calcite is increased prominently, which elevates the complexity of creating effective wormholes even with normally slow reacting acids rather than highly reactive ones (Frenier *et al.* 2001).

Hydrochloric acid has been the most used acid in the oil and gas industry for acidizing conventional wells in carbonate formations of low temperatures, for its high dissolution capability and relatively low cost. The setbacks of the high reaction rate between acid and rock, and the corrosion of tubulars and downhole equipment, raise critical concerns during acid stimulation treatments. These complications are further amplified in the cases of high temperatures and deep reservoirs. Emulsified acid, where the acid is mixed and coated with a hydrocarbon phase at a certain ratio, has been employed as a retarded form of a strong acid. One of the eminent emulsified acids is HCl-in-diesel emulsified acid. The diesel phase protects tubulars from corrosion and the formation from reacting

vigorously with HCl. Several studies have been conducted to optimize the emulsified acid to get the best penetration and wormholing (Al-Mutairi *et al*. 2009, Sayed and Nasr-El-Din 2013).

Chelating agents are another technique to achieve optimum wormholing conditions without the risk of corrosion caused by low pH fluids, or face dissolution caused by high reaction rates. These chelating agents have high pH values and slow reaction rates with reported considerable thermal stability. These chemicals react with carbonates gradually and form complexes with metal ions such as Ca^{2+}, Mg^{2+} or Fe^{3+}, depending on their affinity, and keep these cations in solution. Examples of these chelating agents are Ethylenediaminetetraacetic acid (EDTA)(Fredd and Fogler 1998a), L-glumatic acid-N, N-diacetic acid (GLDA) (LePage *et al.* 2009), hydroxyethylenediaminetetraacetic acid (H-EDTA), nitrilotriacetic acid (NTA), hydroxyethyliminodiacetic acid (HEIDA) (Frenier *et al.* 2003), and aminopolycarboxylic acid (APCA) (Reyes *et al.* 2013). According to the literature, each of these chelating agents has its advantages and applications. The wormholes created as a result of reacting chelating agents with calcium carbonate may differ from those created by reacting HCl with carbonate.

In this study, four different stimulation fluids, mainly HCl, an emulsified acid and two chelating agents, have been investigated in terms of wormhole generation and breaking-through (deeply penetrating) core plug samples of similar petrophysical properties. The resulting wormholes clearly reflect the differences between these fluids at the tested conditions. The first objective of this study is to validate the NMR as a wormhole characterization technique and correlate its results with CT scan and coreflooding differential pressure data. The second objective is to determine the performance of the

subject stimulation fluids in generating conductive wormholes through similar core plug samples at similar conditions.

1.1 The Importance of Wormhole Characterization

The significance of wormhole characterization stems from its role in the evaluation and guidance of the design of stimulation treatments. Prior to field implementation, stimulation fluids are often tested and evaluated in laboratories through various stages, including wormhole generation in coreflooding experiments. Depending on the conclusions of the evaluation and/or optimization of these fluids, recommendations of stimulation designs are directed to field implementation. Therefore, the success of any given acid stimulation treatment depends primarily on the initial laboratory assessment as well as the proper field execution.

The efficiency of the wormhole is evaluated by the depth of penetration and the consumed volume to reach that depth. Fredd and Miller (2000) have categorized the wormholes from face dissolution, conical wormhole, dominant wormhole, ramified wormhole, and uniform dissolution, as seen in **Figure 1**. Furthermore, the health of a wormhole is another vital parameter for characterization. In order to avoid collapse or plugging, wormholes should have certain radii to sustain pressure or allow fines to flow through. Optimum wormholes connect the wellbore to the undamaged reservoir rock through the shortest and healthiest path with limited acid consumption.

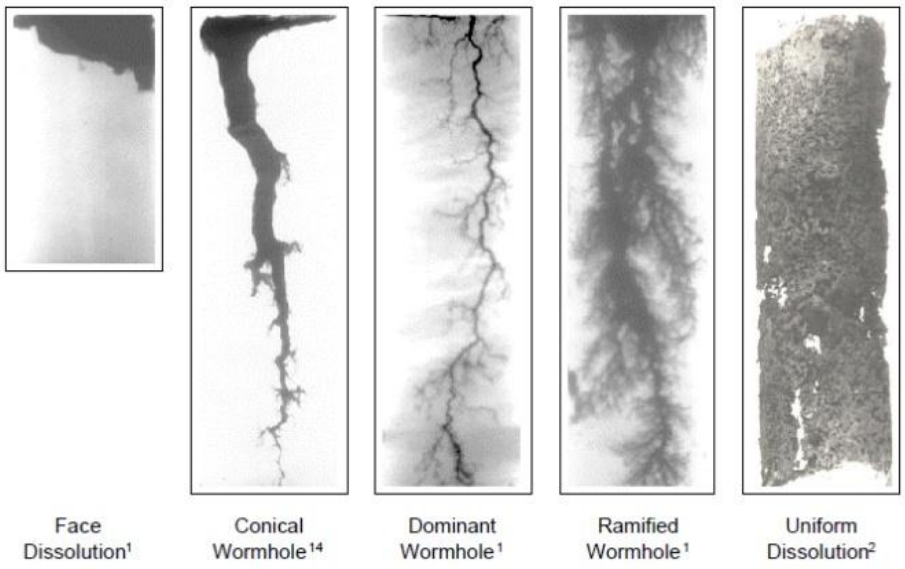

Figure 1: Types of Wormholes (Fredd 2000).

1.2 Nuclear Magnetic Resonance (NMR) as a Characterization Tool for Wormholes

Different tools have been used in the industry to evaluate and characterize wormhole generation. The introduction of NMR as a new characterization tool was an attempt to add a different perspective to increase the comprehension of the factors governing the wormhole generation. Currently, the most used characterization techniques for wormholes are the differential pressure data from coreflooding experiments and computed tomography (CT) scan images of core plugs before and after the introduction of acid.

1.2.1 Coreflooding Differential Pressure Data

Differential pressure data reflect the nature of acid progress inside the core plug sample, indicate the occurrence of a breakthrough, and qualitatively imply the size of wormhole based on the volume of acid consumed. The fluctuation of the differential pressure value also indicates the liberation of CO_2 and the changes in rheological properties of the injected fluid as it reacts with the rock. The breakthrough pore volume (PV_{BT}) is calculated from the starting point of injecting a certain fluid, in this case an acid, to a point where the differential pressure drops dramatically often below the initial level, as seen in **Figure 2**.

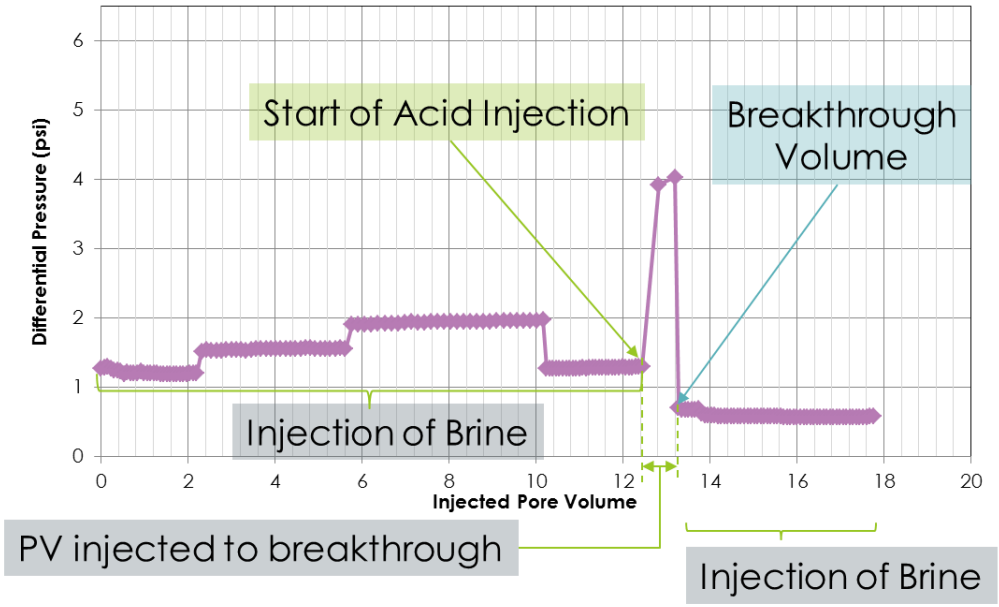

Figure 2: The procedure of calculating the breakthrough pore-volume.

1.2.2 CT Scan

The CT scan provides a graphical representation of density distribution at certain slices along the core plug sample, as seen in the example in **Figure 3**. High density areas are denoted with high CT numbers, and vice versa. Core plug samples should be scanned before and after the introduction of the stimulation fluid for the analysis to be complete. The difference between the two scans is often caused by the rock dissolution as a result of acid injection. The size and path of generated wormholes are very distinctive in the CT scan images and can be measured qualitatively. Further processing of CT scan data can produce visualized representation of the generated wormhole. This representation can lead to further measurements, such as the volume, average diameter and tortuosity of the wormhole. In addition, CT scan can be used to indicate the presence of different lithologies, e.g. calcite and dolomite, inside the core plug sample at high accuracy using the dual energy technique (Siddiqui and Khamees 2004).

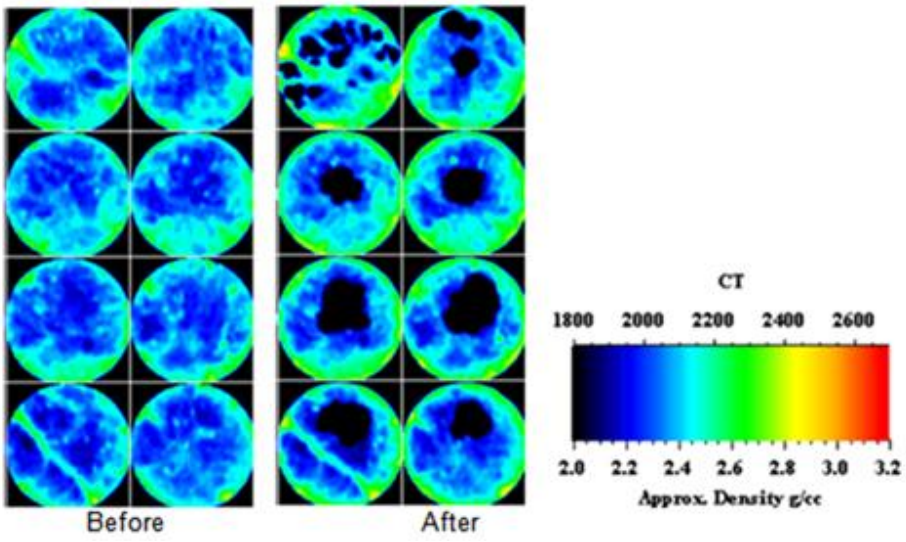

Figure 3: CT slices of core plug sample no. 10 pre- and post-acidizing.

1.2.3 NMR

Nuclear magnetic resonance (NMR) in laboratory and field applications has gained recognition for being one of the most valuable formation characterization tools. Among various NMR applications in the field of geoscience, measurement of the rock porosity, which is independent of mineralogy, became one of the standard tools (Kenyon 1992; Straley 1997). The measured total amplitude of H^1-NMR signal is directly proportional to the total amount of hydrogen nuclei in the sample. Thus, when all the pores inside a porous material are filled with fluids contain proton nuclei, such as water and hydrocarbons, the total amplitude of NMR signal represents the total porosity.

Another well-received NMR application is the determination of pore size distribution by NMR relaxation measurements. The two NMR relaxation times, T_1 (spin-lattice relaxation) and T_2 (spin-spin relaxation) are directly correlated with pore size distribution (Kenyon 1992; Straley 1997; Kleinberg 1994; Sørland 2007). Since T_1 measurement is more time consuming, T_2 measurement is widely used in the modern NMR laboratory and logging application. The principles of NMR T_2 relaxation in porous media can be described as (Korringa 1962):

$$\frac{1}{T_2} = \frac{1}{T_{2B}} + \rho\frac{S}{V} + \frac{D}{12}(\gamma G \tau_e)^2 \quad (8)$$

where $1/T_{2B}$ is the bulk relaxation rate, S/V is the surface area to the volume ratio of pores, ρ is the surface relaxivity, D is the molecular self-diffusivity, G is the magnetic field gradient, γ is the gyromagnetic ratio of proton, and τ_e is the echo delay time. Under fast diffusion regime or surface limited regime with low-field NMR, the above equation of T_2 relaxation rate can be approximated by (Kleinberg 1994):

$$\frac{1}{T_2} = \rho \frac{S}{V} \quad (9)$$

Thus, the geometrical parameters of pores, *S/V*, can be derived from T_2 relaxation rate. If specific surface relaxivity (ρ) of the pore is known, the accurate determination of pore body size is also possible.

The direct relationship between NMR relaxation time and pore size distribution mentioned above breaks down in pore system with complicated connectivity between different pore types, such as micro- and macro-pores in carbonates. Due to the diffusion of magnetization, called diffusion coupling, between various pore types, the determination of pore sizes from NMR relaxation times from multi-modal porosity system is non-trivial (Freeman 1999; Toumelin 2002; Grunewald 2011; Toumelin 2003; Ramakrishnan 1998). **Figure 4** shows two bi-model pore systems with different connectivity. When two types of pores are completely isolated, the T_2 time is directly related to the pore body size. When they are, however, connected to each other, T_2 distributions are getting close to

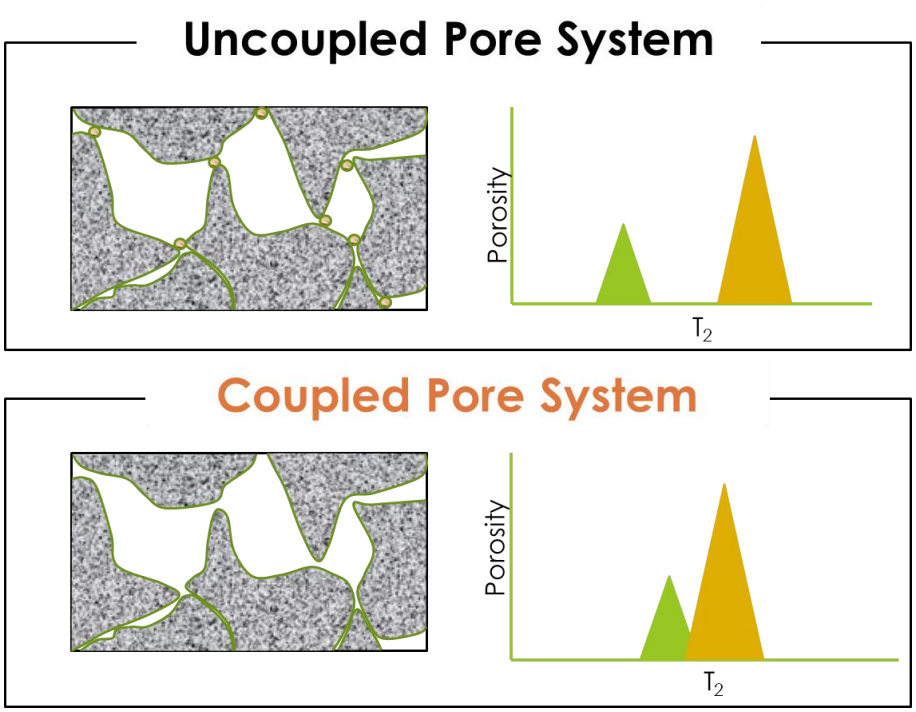

Figure 4: Two bi-modal pore systems with different connectivity

each other. In this case, T_2 time fail to determine true pore body size unless the connectivity is known. The measured total amplitude of H^1-NMR signal is directly proportional to the total amount of hydrogen nuclei in the sample. Thus, when all the pores inside a porous material are filled with fluids contain proton nuclei, such as water and hydrocarbons, the total amplitude of NMR signal represents the total porosity.

2 Chapter 2

EXPERIMENTAL PROCEDURE AND STUDY

PREPARATIONS

2.1 Core Plug Preparations

Core plug samples from Formation X were received after they were cleaned (leached), and the permeability, porosity and grain density were measured. In addition, a set of core plug samples from Indiana limestone were measured for petrophysical properties. The dimensions (length and diameter) were measured to calculate the bulk and pore volumes. The petrophysical properties, dimensions and volumes of the subject core plug samples are presented in **Table 1**. In addition, core plug samples were analyzed semi-quantitatively using XRD. **Table 2** shows the results of the XRD analysis of these samples.

Table 1: Petrophysical properties, dimensions and volumes of core plug samples.

Core sample #	Porosity %	Permeability, md	Length, inch	Diameter, inch	Pore Volume, cc	Source
1	9.2	34.2	1.81	1.49	4.76	Carbonate Formation X
2	15.5	19.4	1.80	1.49	7.97	
3	13.8	2.9	1.811	1.493	7.17	
4	11.1	2.6	1.904	1.502	6.14	
5	20.7	9.9	1.715	1.495	10.21	
6	22.4	8.2	1.715	1.488	10.95	
7	20.3	7.8	1.824	1.488	10.56	
8	10.1	29.3	1.76	1.49	5.08	
9	22.3	76.1	1.79	1.49	11.41	
10	22.8	7.3	1.835	1.498	11.02	
11	20.2	7.8	1.835	1.488	10.56	
12	18.5	6.1	1.83	1.49	11.25	
13	21.1	5	1.925	1.493	11.65	
14	17.5	2.4	1.763	1.494	8.86	
25	16.17	3.18	1.917	1.495	8.92	Indiana Limestone
26B	16.97	2.67	2.009	1.494	9.79	
26	16.27	2.43	1.91	1.491	8.89	
25B	16.61	3.21	1.93	1.494	9.21	

Table 2: XRD semi-quantitative analysis of some of the core plug samples.

Core sample #	Calcite, wt%	Dolomite, wt%	Quartz, wt%	Depth, ft
1	-	-	-	6768.5
2	-	-	-	6573.5
3	73.1	26.4	0.5	7304.7
4	-	-	-	7036.7
5	87.3	12.5	0.2	7298.2
6	82.4	17.4	0.2	7291.8
7	89.5	10.5	Trace	7297.2
8	-	-	-	6712.5
9	-	-	-	6595.5
10	84.4	15.4	0.2	7292.3
11	74.3	25.7	Trace	7279.8
12	-	-	-	7298.7
13	79.4	20.6	Trace	7279.3
14	72.4	27.6	Trace	7280.3
25	99	-	1.0	-
26B	99	-	1.0	-
26	99	-	1.0	-
25B	99	-	1.0	-

2.2 CT Scan Experimental Procedure

Core plug samples in dry condition were non-destructively scanned using X-ray Computed Tomography (CT) scanner at 5 mm intervals starting at 3 mm from the inlet face of the plug towards the outlet face before and after the acid treatment. A total of average of 8 slice images for each plug samples was obtained. The resolution of the images obtained was 100 μm. Since the CT scanning was performed at the same locations for each plug samples (before and after the acid treatment), a direct comparison of the effect of the acid treatment was possible. In fact, this is of a great contribution in evaluating the efficiency of the acid treatment on the rock samples.

Figure 3 shows the CT slice images of core plug sample no. 10 pre- and post-acidizing. As the density scale specifies, the color becomes darker as the CT number, or grain density, becomes smaller. In addition, slices in the pre-acidizing stage might indicate the presence of initial vugs, porous media, or even different mineralogy, depending on the CT resolution. In the post-acidizing stage, the slices contain more dark areas than in the pre-acidizing stage, which reflects the creation of new porous areas as a result of acid injection and rock dissolution. Also, the path of the wormhole might confirm the presence of a low-density path which the acid/stimulation fluid preferably would follow as the opposing pressure becomes less.

2.3 NMR Experimental Procedure

The T_2 relaxation time measured by the Carr-Purcell-Meiboom-Gill (CPMG) sequence method provides information about the fluid saturation, pore structure, and surface chemistry alteration during core-flooding experiments. CPMG however, does not provide

site specific information. In other words, CPMG only provides a lump sum response of T_2 relaxation from a given sample. Samples were saturated in 3 wt.% KCl brine prior to analysis. Samples were analyzed with and without the use of the Teflon mold (tube). The inner diameter of the Teflon tube is 1.503 inch, which was large enough to insert the samples and small enough to minimize the interference of the water residing between the samples and the inner wall.

3 CHAPTER 3

LITERATURE REVIEW

3.1 HCl and Emulsified Acid

The literature is rich with discussions and debates about carbonate acidizing and acid systems. It has been reported in the literature (Kalfayan 2008) that HCl was first used for oil wells stimulation from carbonate formations in Lima, Ohio in 1895. However, it was only after almost a century when emulsified acid was first used to acidize the carbonate matrix in 1985 (Hoefner and Fogler 1985, Hoefner *et al.* 1987, Navarrete *et al.* 1998). Acid in micro-emulsion was then investigated in terms of its viscosity, diffusion rate, spent pore volumes, and created wormhole efficiency (Hoefner *et al.* 1987). Emulsified acids are mainly constrained by temperature, at which the emulsion stability is at risk. In addition, several emulsified acid systems have been studied and their performances were compared to live HCl acid in terms of injection rate, viscosity and thermal stability (Buijse and van Domelen 1998). The use of emulsified acid in core plug samples with tar saturation was of a less advantage than that of samples with water saturation (Al-Mutairi *et al.* 2012). It was also concluded in this study that breakthrough pore volume in rock saturated with intermediate oil was less than that of condensate saturation. Sayed *et al.* (2012) have recently introduced a new emulsifier that can withstand temperatures up to 300 °F and exhibit rheological properties better than those of the widely used commercial

emulsifiers. Rotating disks were used to determine the reaction rate between emulsified acid and rock, and coreflooding experiments to investigate its wormholing efficiency.

3.2 Chelating Agents

EDTA has been discovered to be effective to create wormholes in limestone at pH range of 4-13 (Fredd and Fogler 1998a). They stated that EDTA and acetic acid (HAc) stimulated limestone more efficiently than HCl at rates greater than 0.1 cm^3/min, where the latter created face dissolution. In another study, it was determined that the structure and permeability response of wormholes created by injection chelating agents into calcite are dependent on Damköhler number (Fredd *et al.* 1997), which is defined as the ratio of the rate of dissolution by acid to the rate of convective transport of acid. As the Damköhler number is decreased, the amount of wormhole branching increases when injecting calcite with chelating agents such as cyclohexanediaminetetraacetic acid (CDTA) and diethylenetriaminepentaacetic acid (DTPA). Acetic acid and EDTA were compared to long-chained carboxylic acid (LCA) at high temperatures (Huang *et al.* 2003). It was found that LCA can be injected at lower rates than EDTA and acetic acid. In addition, LCA created smaller wormholes than that by HAc and EDTA at the optimum rates. GLDA and HEDTA were studied and compared to HCl (Mahmoud *et al.* 2011). The study concluded that GLDA and HEDTA, unlike HCl, did not cause face dissolution at low injection rates. In addition, GLDA was more efficient at high temperatures than HEDTA or HCl.

Chelating agents react with calcium carbonate in a different mechanism. EDTA, as an example of chelating agents, undergoes a stepwise loss of protons to reach the fully ionized state, as shown in Equations 2-5 (Fredd and Fogler 1998b):

$$H_4Y \leftrightarrow H_3Y^{-1} + H^+ \tag{2}$$

$$H_3Y^{-1} \leftrightarrow H_2Y^{-2} + H^+ \tag{3}$$

$$H_2Y^{-2} \leftrightarrow HY^{-3} + H^+ \tag{4}$$

$$HY^{-3} \leftrightarrow Y^{-4} + H^+ \tag{5}$$

where H_4Y represents EDTA. Li *et al.* (2008) discussed in detail the chelation chemistry and the interfacial reactions. Reactions at the solid-liquid interface include water attack, proton attack and ligand attack, which are detailed below:

Water Attack:

$$H_2O_{(i)} + CaCO_3 \leftrightarrow OH^-_{(i)} + Ca^{2+}_{(i)} + HCO^-_{3(i)} \tag{6}$$

Proton Attack:

$$H^+_{(i)} + CaCO_3 \leftrightarrow Ca^{2+}_{(i)} + HCO^-_{3(i)} \tag{7}$$

$$H_4L_{(i)} + CaCO_3 \leftrightarrow H_3L^-_{(i)} + Ca^{2+}_{(i)} + HCO^-_{3(i)} \tag{8}$$

$$H_3L^-_{(i)} + CaCO_3 \leftrightarrow H_2L^{2-}_{(i)} + Ca^{2+}_{(i)} + HCO^-_{3(i)} \tag{9}$$

$$H_2L^{2-}_{(i)} + CaCO_3 \leftrightarrow HL^{3-}_{(i)} + Ca^{2+}_{(i)} + HCO^-_{3(i)} \tag{10}$$

$$HL^{3-}_{(i)} + CaCO_3 \leftrightarrow L^{4-}_{(i)} + Ca^{2+}_{(i)} + HCO^-_{3(i)} \tag{11}$$

where H_4L represents a chelating agents such as EDTA.

Ligand Attack:

$$L^{4-} + CaCO_3 \leftrightarrow CaL^{2-} + CO_3^{2-} \quad (12)$$

$$HL^{3-} + CaCO_3 \leftrightarrow CaHL^{-} + CO_3^{2-} \quad (13)$$

$$H_2L^{2-} + CaCO_3 \leftrightarrow CaH_2L + CO_3^{2-} \quad (14)$$

The water/ligand attack controls the reaction rate for high pH, while the proton attack controls the reaction rate at low pH (Fredd and Fogler 1998b). At high pH, the dissolution process consists of the adsorption of deprotonated chelating ions on the surface, the complexation and the desorption of calcium complex and carbonate products. The process becomes as follows:

$$L^{4-} \leftrightarrow {L^{4-}}_{(ads)} \quad (15)$$

$${L^{4-}}_{(ads)} + CaCO_3 \leftrightarrow {CaL^{2-}}_{(ads)} + {CO_3^{2-}}_{(ads)} \quad (16)$$

$${CaL^{2-}}_{(ads)} \leftrightarrow {CaL^{2-}}_{(i)} \quad (17)$$

$${CO_3^{2-}}_{(ads)} \leftrightarrow {CO_3^{2-}}_{(i)} \quad (18)$$

where *ads* and *i* indicate adsorbed species at the surface, and species located at the solid-liquid interface, respectively.

3.3 NMR as an Analytical Tool for Wormholes

Nuclear magnetic resonance (NMR) was first discovered in 1945 by two independent research groups (Purcel *et al.*, 1945; and Bloch *et al.*, 1946) (Akkurt *et al.*, 2009). NMR was then recognized as a potential analytical tool in the 1950s, which lead to the development of nuclear magnetic logging (NML) in the 1960s (Freedman 2006). In 1978, Wyman introduced the first commercial NMR tool (Akkurt *et al.*, 2009).

Laboratory studies of flow in porous media using NMR was first done in 1965 by Saraf and Fatt (1967). They were able to measure two- and three-phase relative permeability values of Boise sandstone core plug samples by using NMR technique for measuring fluid saturations. Edelstein *et al*. (1988) have used NMR to measure several petrophysical properties such as porosity and oil/water saturations. They have recommended the use of NMR to conduct petrophysical analysis on core plug samples over the use of conventional core analysis, which were done at a slower pace than NMR analysis. Doughty and Maerefat (1989) investigated the modification of NMR spectrometer for imaging capabilities of water in different sandstone samples. They suggested that higher magnetic field was not always the best option for petrophysical analysis using NMR. Kubica (1995) has compared the permeability and porosity values of sandstone core plug samples obtained from conventional core measurements and Laboratory NMR spectrometer. The study found a valid correlation between the permeability values obtained from the two sources, with a possibility of improving the NMR calibration to increase the accuracy of the permeability estimates. Ohen *et al*. (1996) studied NMR relaxometry for NMR log calibration to enhance petrophysical measurements for

downhole equipment in oil wells. They showed that laboratory NMR instrument, which provides transverse relaxation characteristics of water, can provide the same information as the NMR logging tool, which provides longitudinal relaxation characteristics. In addition, they established that the abundance of micro- to macro-porosity can be concluded from NMR relaxation time distributions.

The influence of pore scale heterogeneities on carbonate stimulation has been studied (Ziauddin 2007). Although NMR has been used in the study, the objective was to characterize the rock's mineralogy, texture, fabric, porosity and density distribution, but not the wormhole formation. CT and geostatistics have been used to characterize the fine-scale heterogeneity, and a connected component-labeling algorithm to characterize the large-scale heterogeneity in carbonate (Izgec 2008). This study reported that acid follows the path of the spatially correlated permeability in addition to the high permeability path. In addition, it was discovered that the connectivity between the vugs is a major factor in determining the path of wormhole. Darcy-Brinkman formulation, which is a coupled Darcy and Stokes flow Principles, has been used to understand and model the wormhole path and acid breakthrough in vuggy carbonate (Izgec 2009). They have concluded that the localized pressure drops created by vugs dominates the flow of acid more than the chemical reaction at the pore level. It has been stated that the fraction of vugs in the total porosity is inversely proportional to the acid breakthrough volume. The modeling and digital visualization of flow through wormholes in acid-stimulated carbonate rock has been investigated (Valsecchi 2012). Experimental, imaging and modeling techniques have been conducted to understand the structure and fluid flow impacts of wormhole

networks formed during acidizing. The targeted parameters were the completion type, saturating fluid, rock type, and acid injection rate.

4 CHAPTER 4

RESULTS AND DISCUSSION

4.1 Comparison between Different Stimulation Fluids

The results of coreflooding results varied depending on the acid systems, injection rates, and pH values. **Table 3** shows the conditions and results of each test.

Table 3: Coreflooding experiments conditions and results using different stimulation fluids, injection rates, pH values and pressure*.

	Stimulation Fluid	Core plug no.	Injection Rate cm^3/min	pH	Back Pressure, psi	PV	
						Injected	Breakthrough
1	15% HCl	1	0.5	0	500	18	No Breakthrough
2		2	1	0	500	14.5	14.5
3	Emulsified Acid (15% HCl)	3	0.5	0	1000	0.5	0.5
4		4	1	0	1000	0.8	0.8
5		5	2	0	1000	0.8	0.8
6	Chelating Agent I (20 wt%)	6	0.5	3-4	1000	18.5	No Breakthrough
7		7	1	3-4	500	15	No Breakthrough
8		8	1	3-4	500	52	No Breakthrough
9		9	1	3-4	1000	12	No Breakthrough
10		10	2	3-4	1000	7.8	7.8
11		11	3	3-4	500	5.1	5.1
12		12	1	13	1000	4.1	5.1
13	Chelating Agent II (20 wt%)	13	1	13	1000	1.2	1.2
14		14	1	3.5	1000	8.1	8.1

* All experiments were conducted at 200˚F and 1,500 psi confining pressure.

4.1.1 Acid Systems

4.1.1.1 Hydrochloric Acid (HCl) at 0.5 and 1 cm^3/min

HCl was used to stimulate the core plug samples at two rates: 0.5 and 1 cm^3/min. **Figures 5 and 6** show the differential pressure obtained from the coreflooding experiments. The differential pressure increased with the introduction of acid into the core plug sample. Since the lithology of the core plug sample contains anhydrite, there is a possibility that it was dissolved by HCl, and then re-precipitated with the increase in $CaCl_2$ concentration, a product of the reaction between HCl and calcium carbonate. This might have resulted in plugging the pores of the core plug, as seen in 5, which created a seal against the injection of acid. As a result, the increase in pressure, after ~64 PV, was due to the compression of injected fluid. In Figure 6, the increase was due to the liberation of carbon dioxide (CO_2) as a product of the reaction of HCl with calcite. The produced CO_2 existed in a free gas form, since the pore pressure was below its critical pressure (~1100psi), which created a new relative permeability and resulted in the reduction of liquid permeability. Although a breakthrough was only achieved when a 1 cm^3/min injection rate was used, the consumed PV is considered very high and ineffective. The face dissolution has been observed from the inlet of the core plug sample as can be seen from **Figure 7.** Since HCl is a strong acid with extremely high reactivity towards calcium carbonate, the injection rate is considered the dominating factor which controls the progress of breakthrough. Therefore, injection rate has to be increased to compete with the reaction rate between HCl and calcium carbonate, which can lead to a breakthrough at a reasonable PV_{BT}.

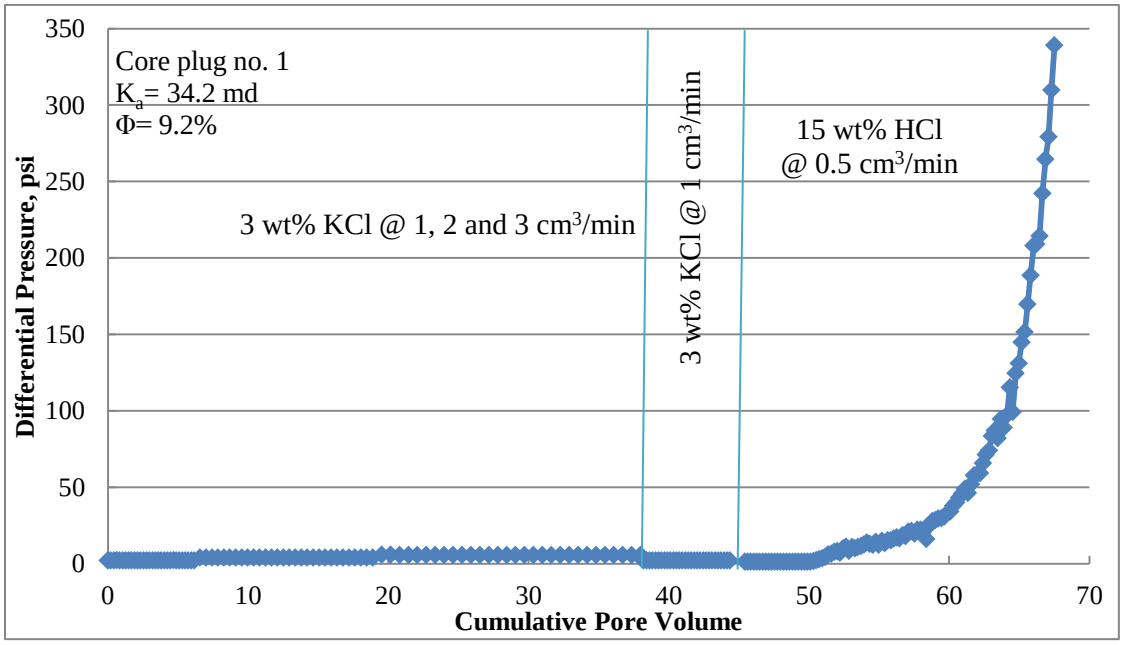

Figure 5: Coreflooding performance of 15 wt% HCl at 0.5 cm^3/min and 200°F.

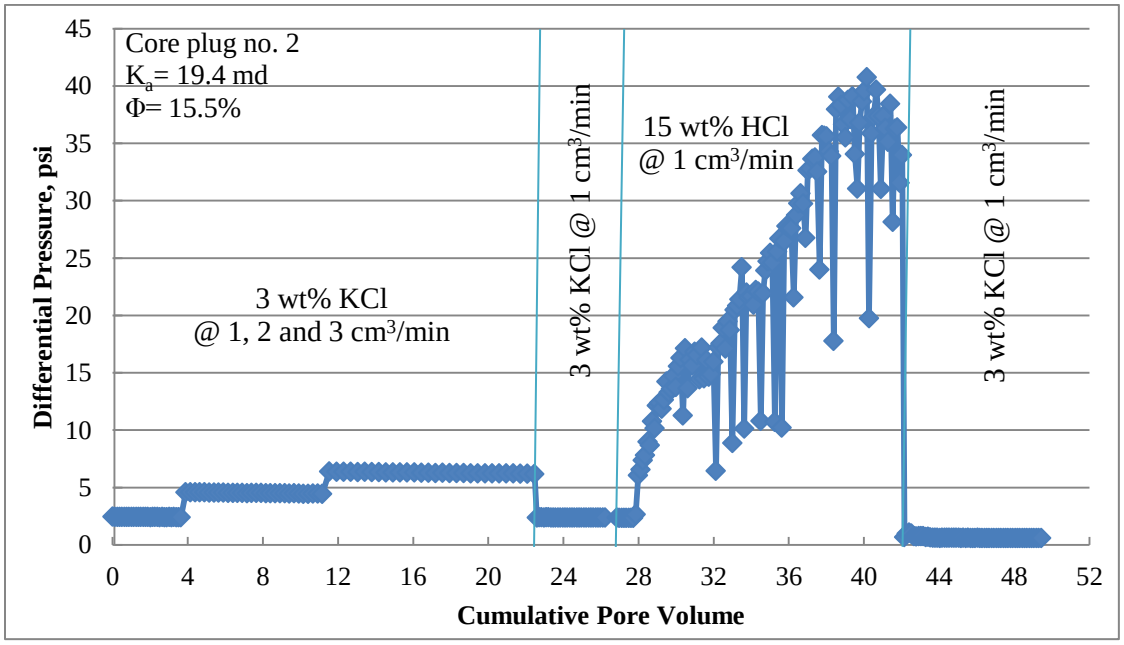

Figure 6: Coreflooding performance of 15 wt% HCl at 1 cm^3/min and 200°F.

Figure 7: Core plug no. 2 after injection of 15 wt% HCl at 1 cm^3/min

4.1.1.2 Injection of Emulsified Acid at 0.5, 1 and 2 cm^3/min

An emulsified acid, made from 70 v% HCl (15 wt%) and 30 v% diesel, was injected through core plug samples at different rates (0.5, 1 and 2 cm^3/min). **Figures 8-10** show the differential pressure between the two ends of a core plug sample at different injection rates. In Figure 10, the change in injection rate when switching from brine, at 1 cm^3/min, to emulsified acid, at 2.0 cm^3/min, caused a sudden jump in the differential pressure. Nonetheless, the differential pressure at 2.0 cm^3/min of emulsified acid was identical to that obtained with brine injection at the same rate, Figure 10. The injected emulsified acid slightly increased the differential pressure due to the liberation of carbon dioxide (CO_2) as a reaction product. In these experiments, the pore pressure was set at 1000 psi, which was still below the critical pressure of CO_2. Therefore, CO_2 existed in a free gas form which reduced the permeability of injected fluid, hence the increase in differential pressure. However, the pressure dropped immediately indicating the completion of a breakthrough and the connection between the two ends of the core plug samples. The immediate drop in pressure also reflected the low PV_{BT}. This phenomenon was observed with all employed injection rates, as seen in **11**. Inlets and outlets of the used core plug samples are shown in **Figure 12**. CT scan images of core plug samples no. 3 and 5 show very conductive wormholes (**Figures 13 and 14**). By comparing the pre- and post-acidizing stages, it is strongly possible that the emulsified acid has followed the path of the least density, especially in Figure 13. Furthermore, 3D visualizations of the created wormholes, rendered using the CT scan data, are shown in **Figure 15**. It is worth noting that these visualizations are only for qualitative comparisons as they are not yet standardized.

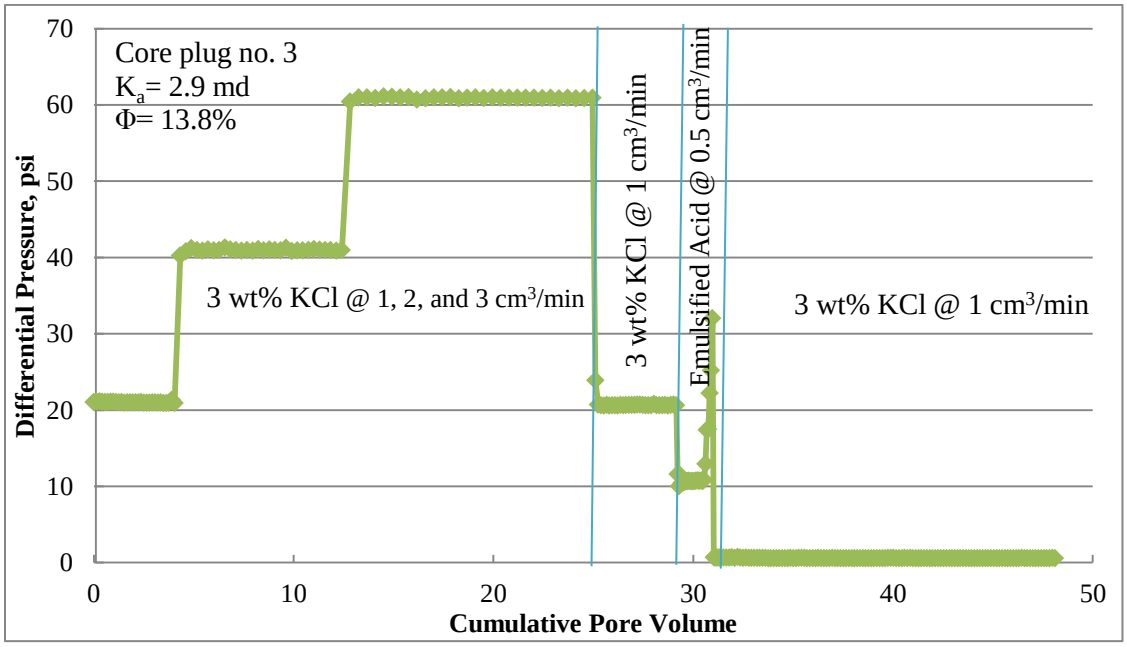

Figure 8: Coreflooding performance of Emulsified Acid at 0.5 cm^3/min and 200°F.

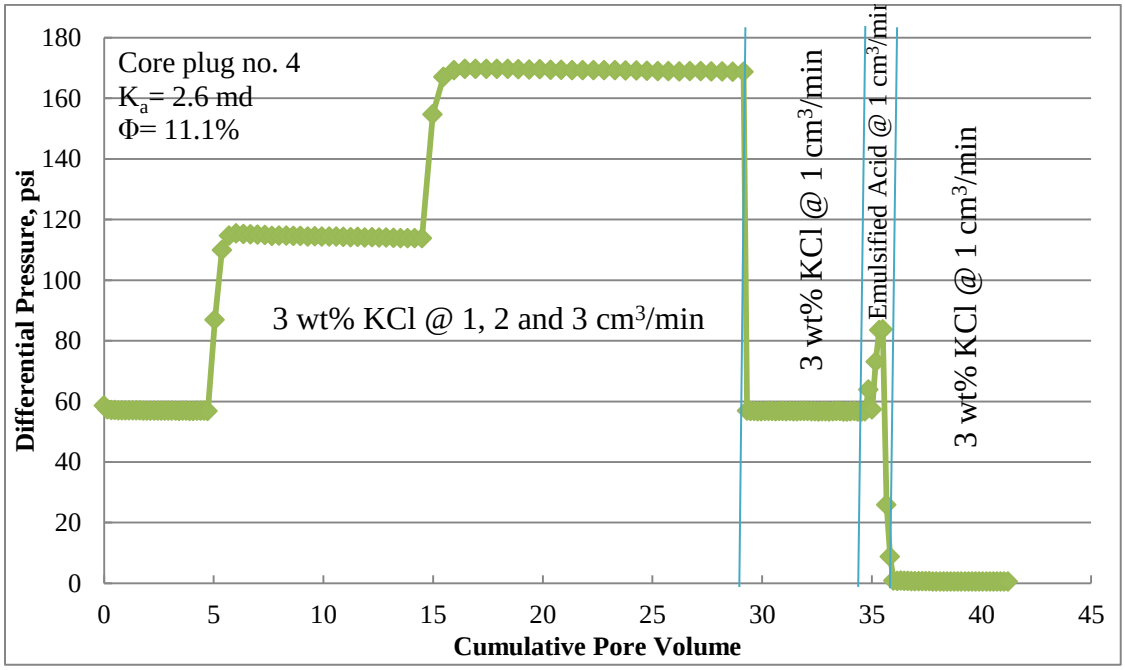

Figure 9: Coreflooding performance of Emulsified Acid at 1 cm^3/min and 200°F.

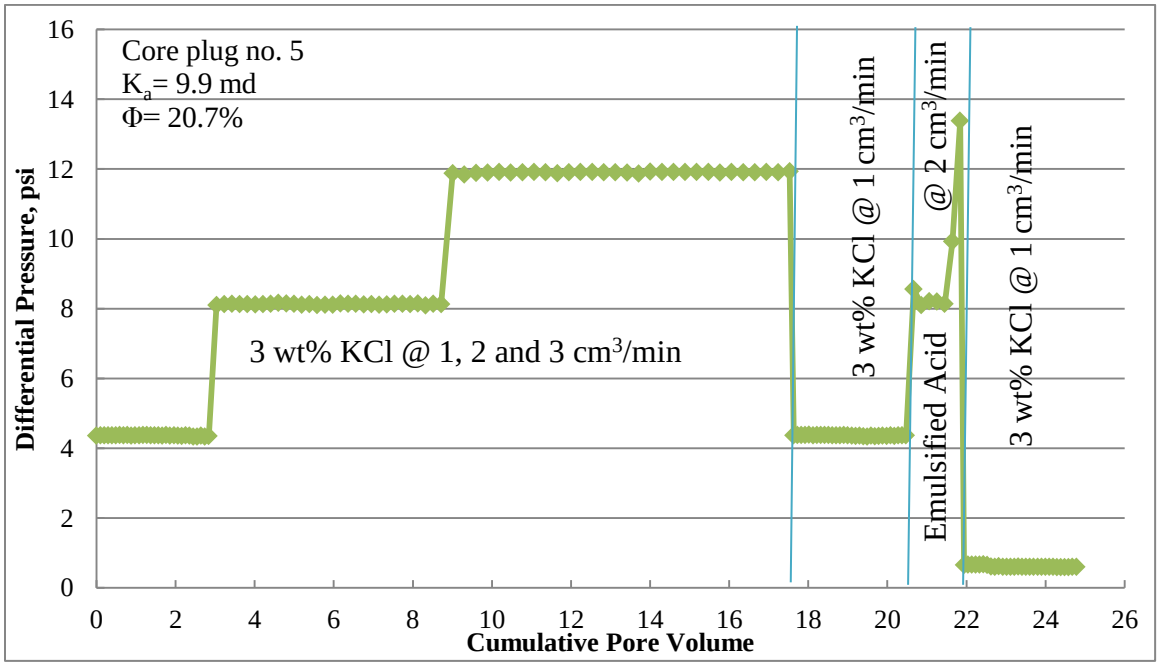

Figure 10: Coreflooding performance of Emulsified Acid at 2 cm^3/min and 200°F.

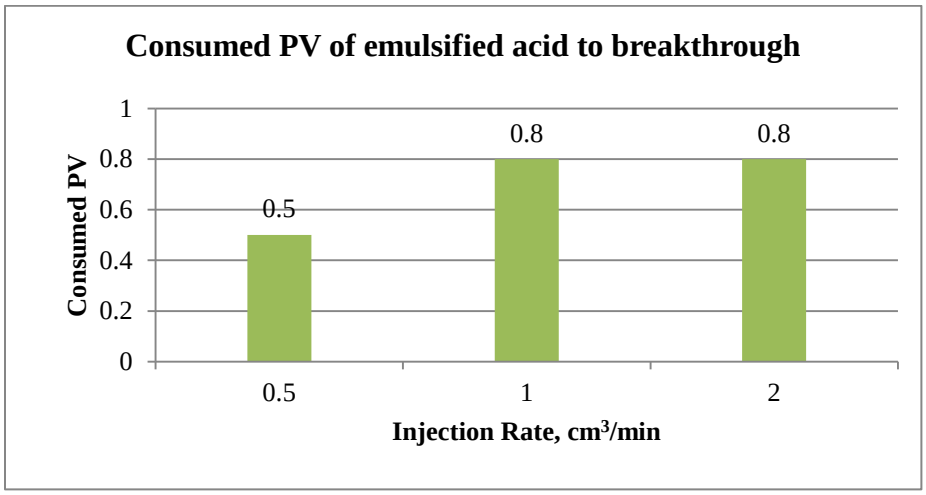

Figure 11: Effect of injection rate on coreflooding performance of emulsified acid.

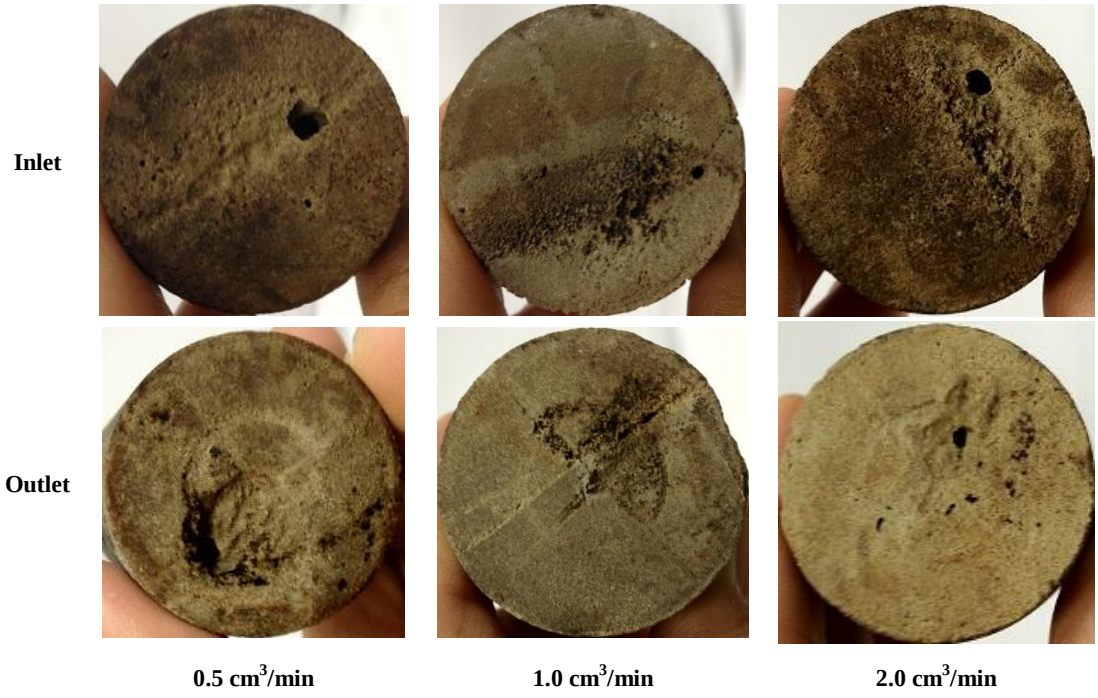

Figure 12: Core plugs no. 3, 4 and 5 after injecting emulsified acid at different rates.

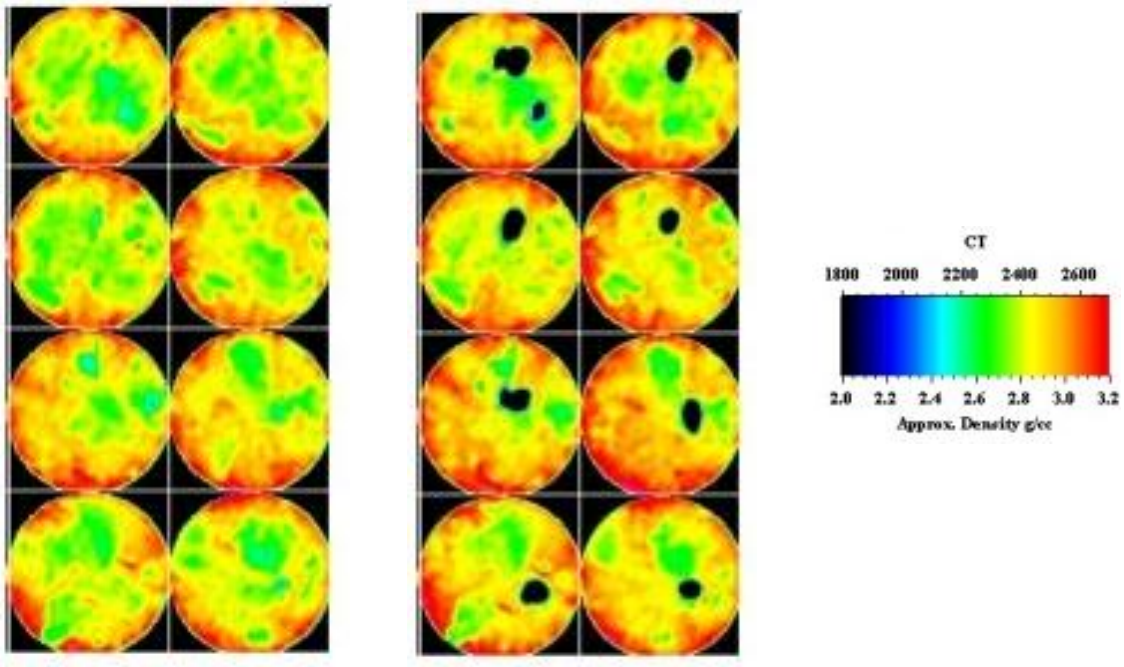

a) before acidizing b) after acidizing c) Density scale

Figure 13: CT Scan analysis of core plug no. 3 (Emulsified Acid at 0.5 cm^3/min).

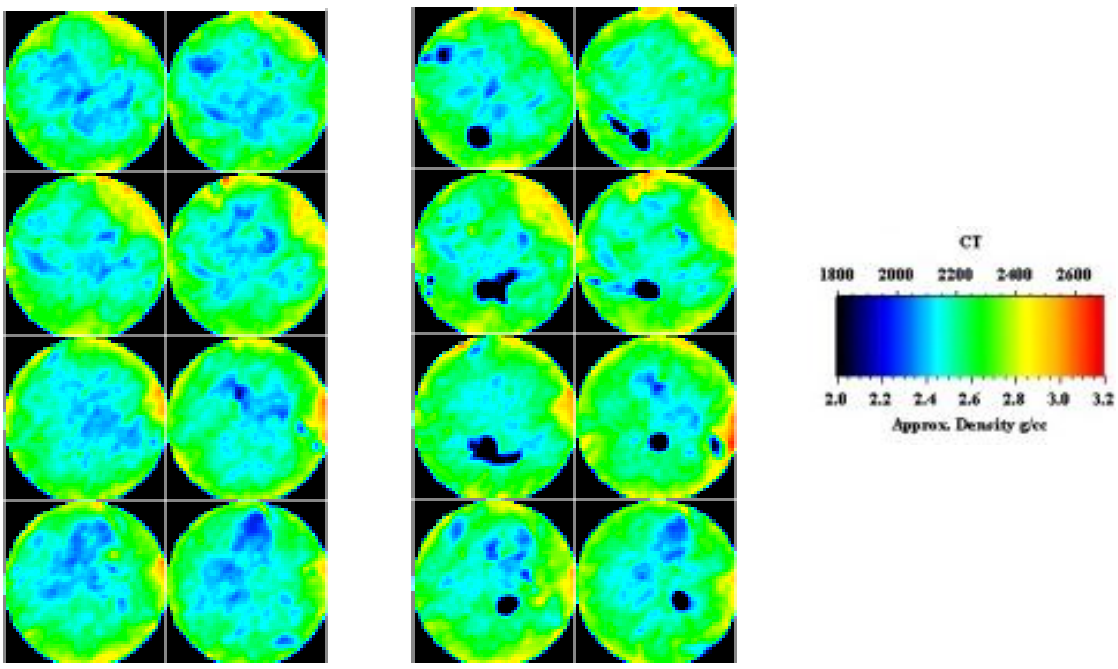

a) before acidizing b) after acidizing c) Density scale

Figure 14: CT Scan images of core plug no. 5 (Emulsified Acid at 2.0 cm^3/min).

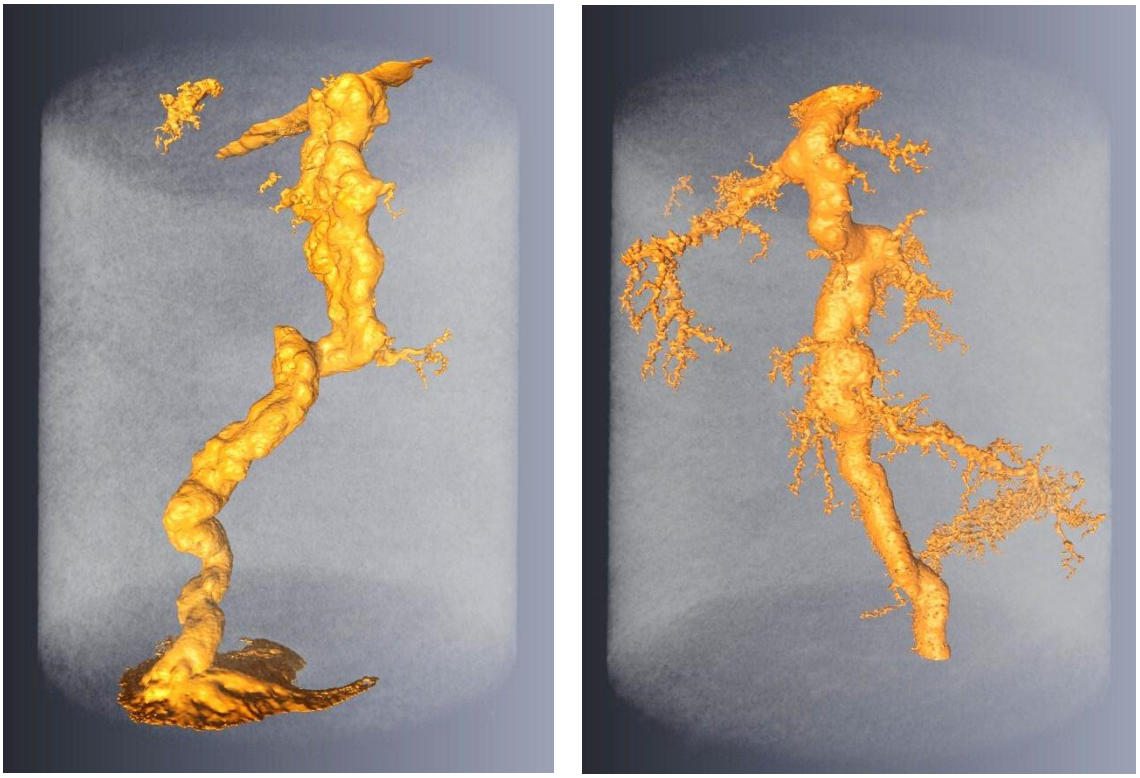

0.5 cm^3/min 2.0 cm^3/min

Figure

Figure 15: 3D visualizations of generated wormholes (Emulsified Acid).

4.1.1.3 Injection of Chelating Agent I at 0.5, 1, 2, and 3 cm^3/min

Several tests have been performed using Chelating Agent I (pH of 3-4) at different injection rates including 0.5, 1, 2, and 3 cm^3/min. Results have varied depending on the employed injection rate.

When 0.5 cm^3/min injection rate was used, the differential pressure increased and reached a plateau during the first 10 PV, as seen in **Figure 16**. After that, the pressure started to decrease gradually and continued for the next 8 PV. However, no breakthrough was achieved after the injection of 18 PV of Chelating Agent 1. The core plug sample was dissolved partially at the inlet face, which indicated face dissolution, as seen in **Figure 17**. The CT scan images further confirmed the manifestation of face dissolution, **Figure 18**. The behavior of Chelating Agent I at this rate was similar to that of HCl, where no face dissolution was observed and a breakthrough was not achieved. **Figure 19** shows a 3D visualization of the dissolved parts of the core plug.

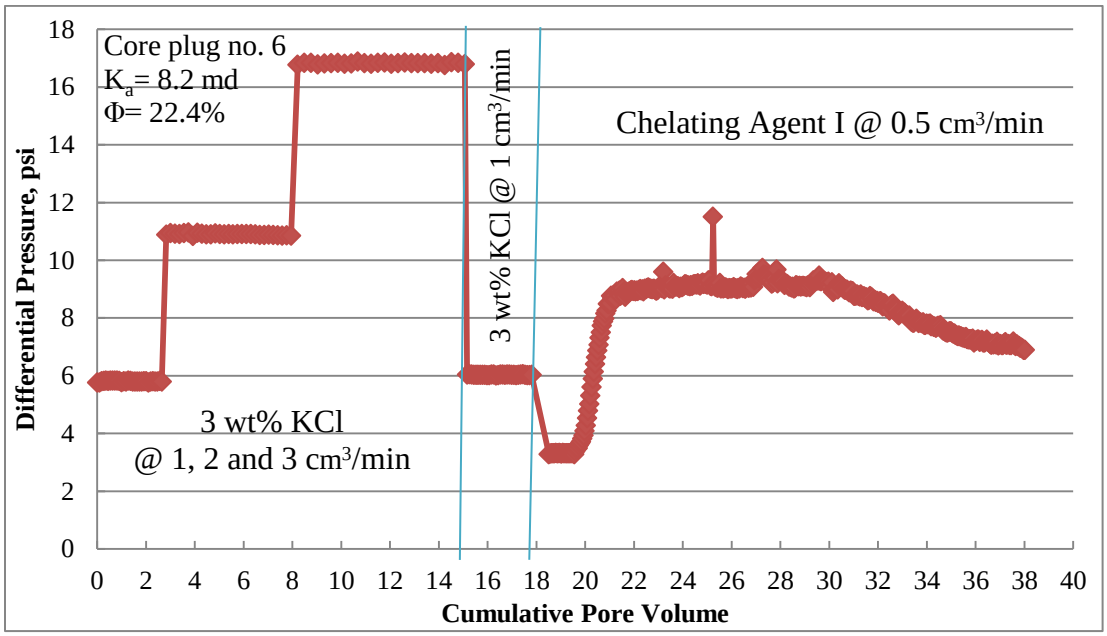

Figure 16: Coreflooding performance of Chelating Agent I (pH 3-4, 0.5 cm^3/min, 200°F).

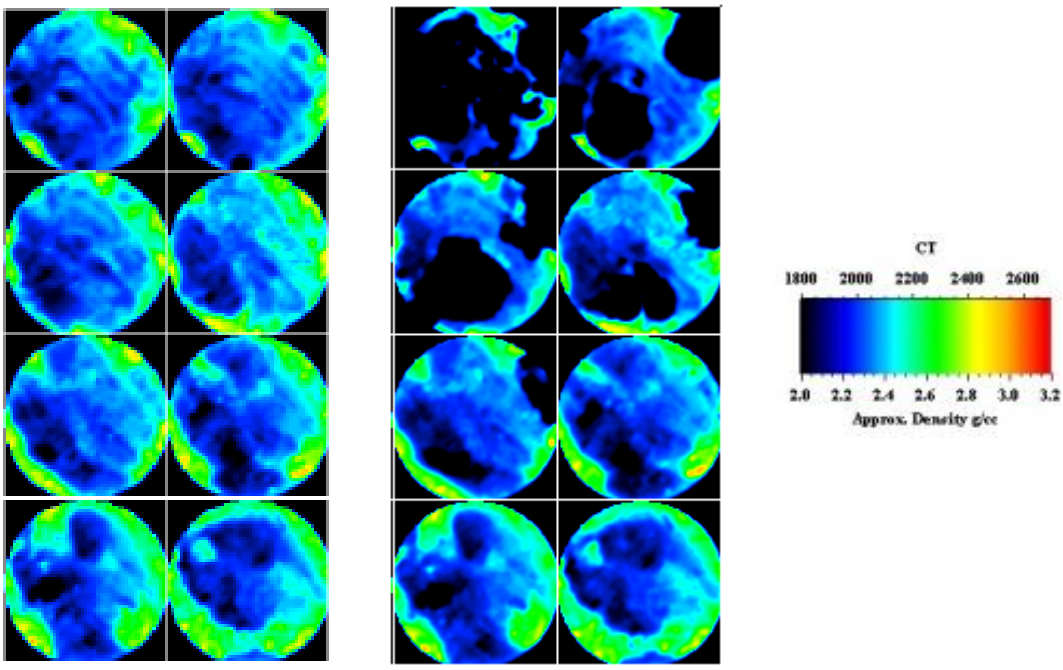

a) before acidizing b) after acidizing c) Density Scale

Figure 17: CT Scan images of core plug no. 6 (Chelating Agent I at 0.5 cm^3/min).

Figure 18: Core plug no. 6 after injecting Chelating Agent I of 0.5 cm^3/min.

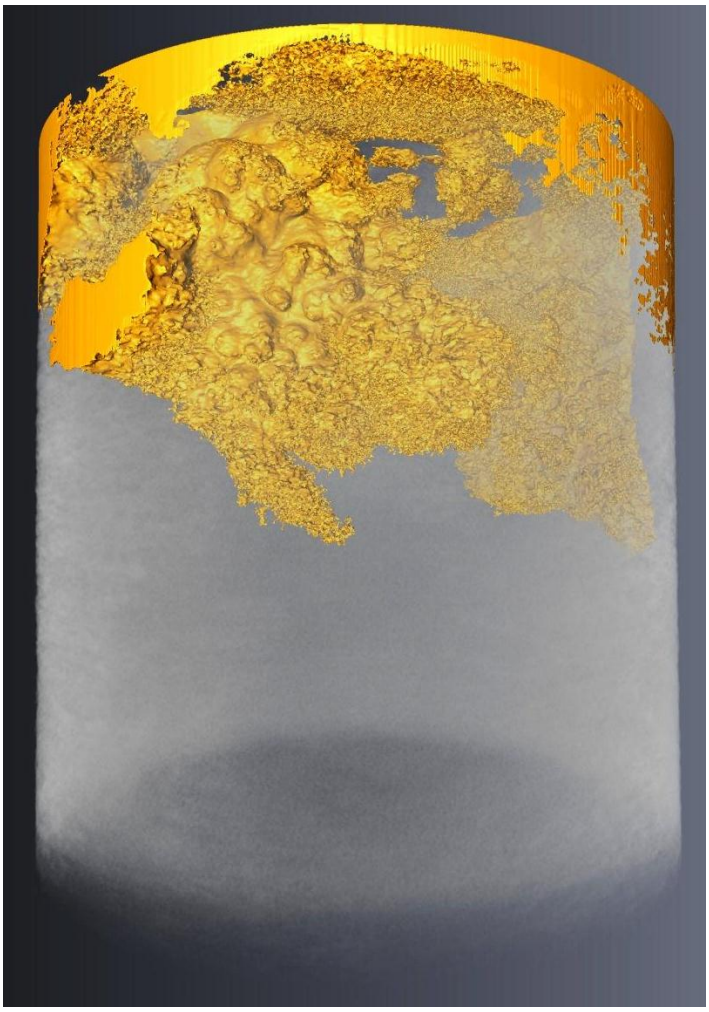

Figure 19: 3D visualizations of dissolution created by Chelating Agent I at 0.5 cm^3/min.

At an injection rate of 1 cm^3/min, a similar behavior was observed, where the pressure increased and plateaued during the injected 15 PV without achieving a breakthrough, **Figure 20**. Face dissolution was observed in the CT scan images and on the core plug sample, as seen in **Figures 21** and **22**. When extracting the core plug sample from the core holder, a mud-like material was observed. This material was analyzed using XRD and it mainly consisted of calcite ($CaCO_3$) and dolomite ($CaMgCO_3$), **Table 4**.

This injection rate was repeated given that it was successful with HCl, even though a high PV_{BT} was consumed. The attempts were executed with minor changes in the back-pressure values as seen in Table 3, and using core plug samples with higher permeability values. The differential pressure data for these attempts are shown in **Figures 23 and 24**. Nevertheless, none of the attempts was successful in achieving a breakthrough using the injection rate of 1 cm^3/min of Chelating Agent I.

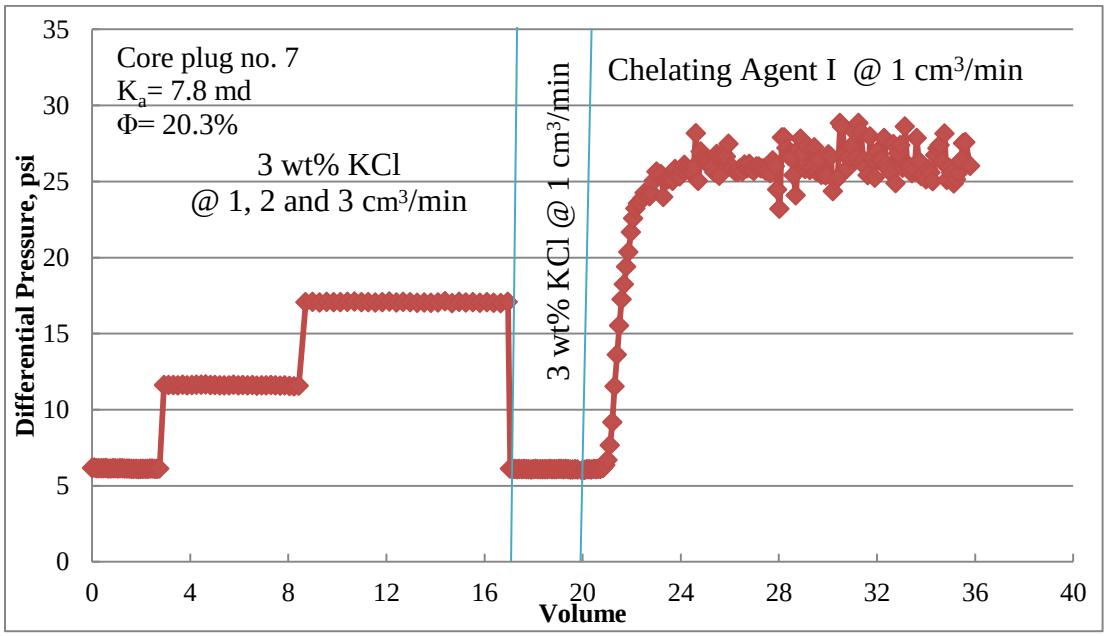

Figure 20: Coreflooding performance of Chelating Agent I (pH 3-4, 1 cm^3/min, 200°F).

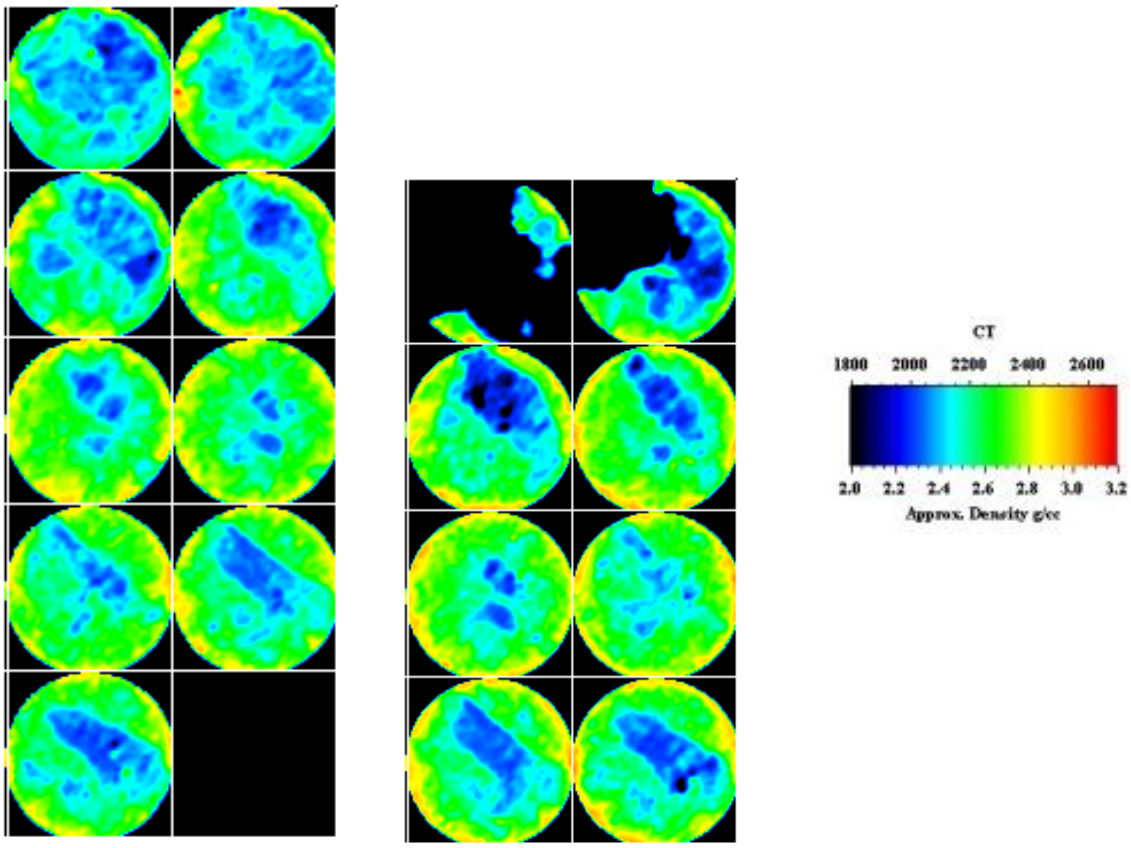

a) before acidizing b) after acidizing c) Density Scale

Figure 21: CT Scan images of core plug no. 7 (Chelating Agent I at 1.0 cm^3/min).

a) b)

Figure 22: a) Core plug no. 7 after injecting Chelating Agent I, and b) Dissolved material found in the core holder after extracting the sample.

Table 4: XRD semi-quantitative analysis of the material produced when Dissolvine StimWell was used at injection rates of 0.5 and 1 cm^3/min.

Component(s)	Concentration, wt%
Calcite-$CaCO_3$	69
Dolomite-$CaMg(CO_3)_2$	31
Quartz-SiO_2	Traces

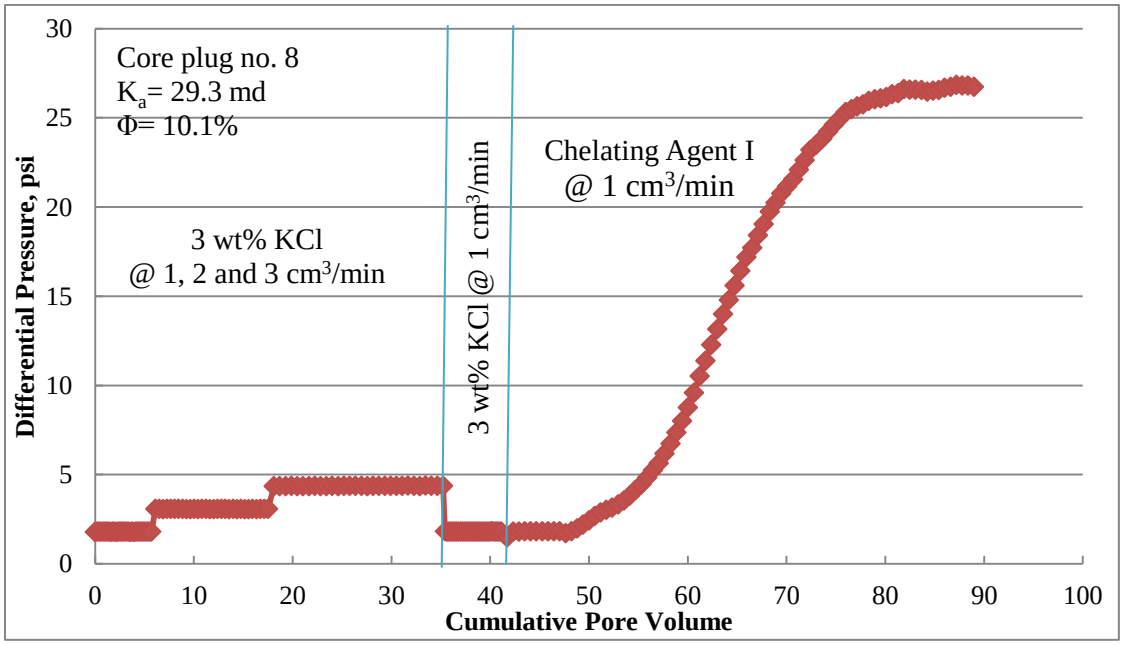

Figure 23: Coreflooding performance of Chelating Agent I (pH 3-4, 1 cm^3/min, 200°F).

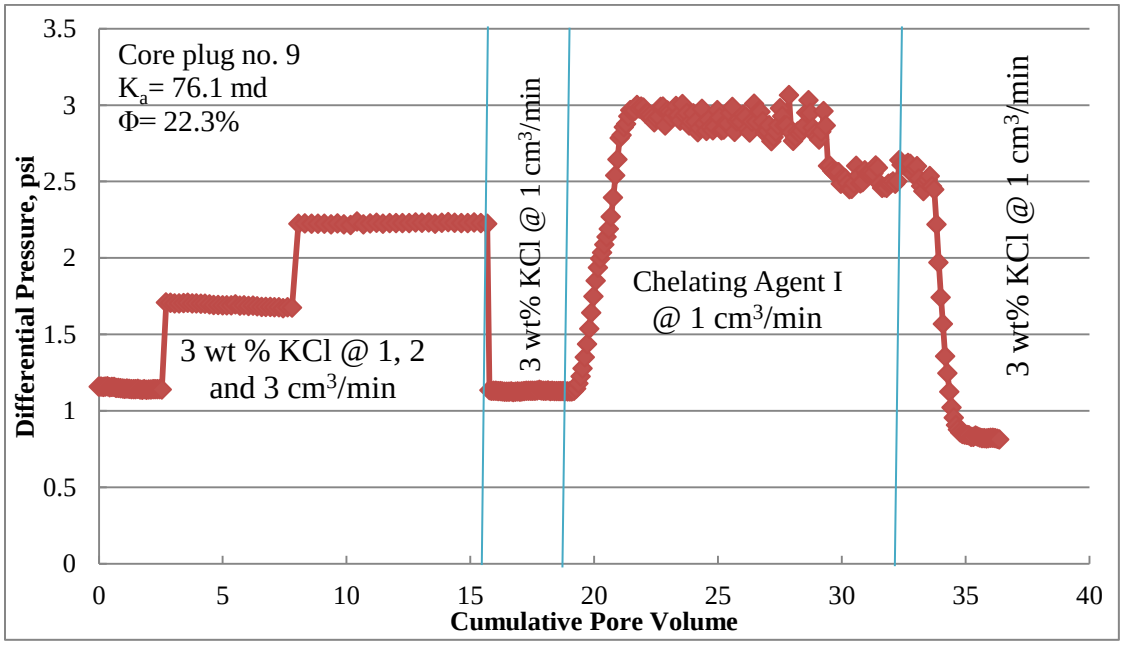

Figure 24: Coreflooding performance of Chelating Agent I (pH 3-4, 1 cm^3/min, 200°F).

When the injection rate was increased to 2.0 cm^3/min, Chelating Agent I was able to achieve a breakthrough after consuming 7.8 PV_{BT}, as seen in **Figure 25**. The relatively high PV_{BT} suggested the generation of a broad wormhole. The CT scan images further confirmed this postulation as seem on **Figure 26**. It is worth mentioning that dissolved material, similar to that found in Figure 22 (b), was observed at a lower quantity.

It is clear that increasing the injection rate has enhanced the performance of Chelating Agent I. However, to confirm this trend, another experiment was conducted using a higher injection rate.

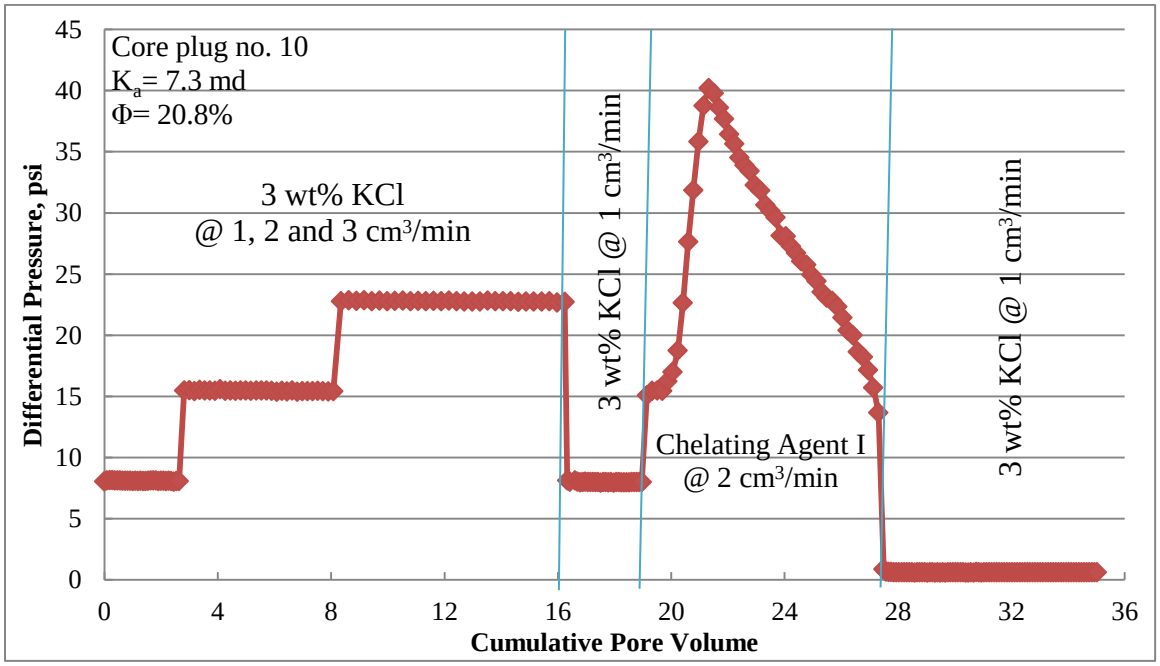

Figure 25: Coreflooding performance of Chelating Agent I (pH 3-4, 2 cm^3/min, 200°F).

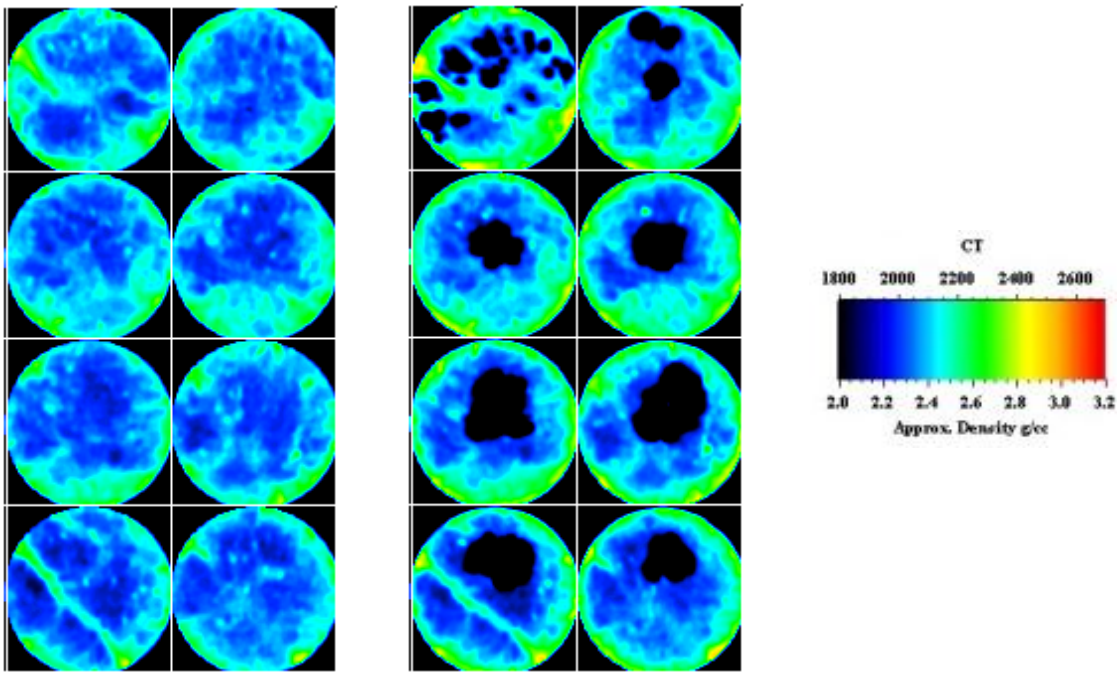

a) before acidizing b) after acidizing c) Density Scale

Figure 26: CT Scan images of core plug no. 10 (Chelating Agent I at 2.0 cm^3/min).

Chelating Agent I was used at an injection rate of 3.0 cm^3/min using core plug sample no. 11. **Figure 27** shows the differential pressure data of this experiment as well as the PV_{BT} at which Chelating Agent I achieved a breakthrough. The CT scan images, **Figure 28**, show a narrower wormhole than that achieved using the injection rate of 2.0 cm^3/min. This confirmed the PV_{BT} of 5.1 calculated from the differential pressure data. In this experiment, only traces of the dissolved material, found in Figure 22 (b), were found in the core holder after extracting the core plug sample.

The breakthroughs of Chelating Agent I at injection rates of 2.0 and 3.0 cm^3/min followed a similar behavior, where the differential pressure increased after the introduction of the stimulation fluid, followed by a gradual decrease in pressure as the chelating agent progressed deeper into the core plug sample. Yet, this behavior is far from optimum where the differential pressure drops instantly, as in Figures 8 - 10, which would result in a small PV_{BT}. **Figure 29** shows a summary of the performance of Chelating Agent I at different injection rates. A 3D visualization of the generated wormholes is shown in **Figure 30**.

Since altering the pressure values did not enhance the performance, the poor functioning of Chelating Agent I may possibly be caused by the lithology of the used core plugs or the employed temperature. The effect of lithology will be discussed later in the study.

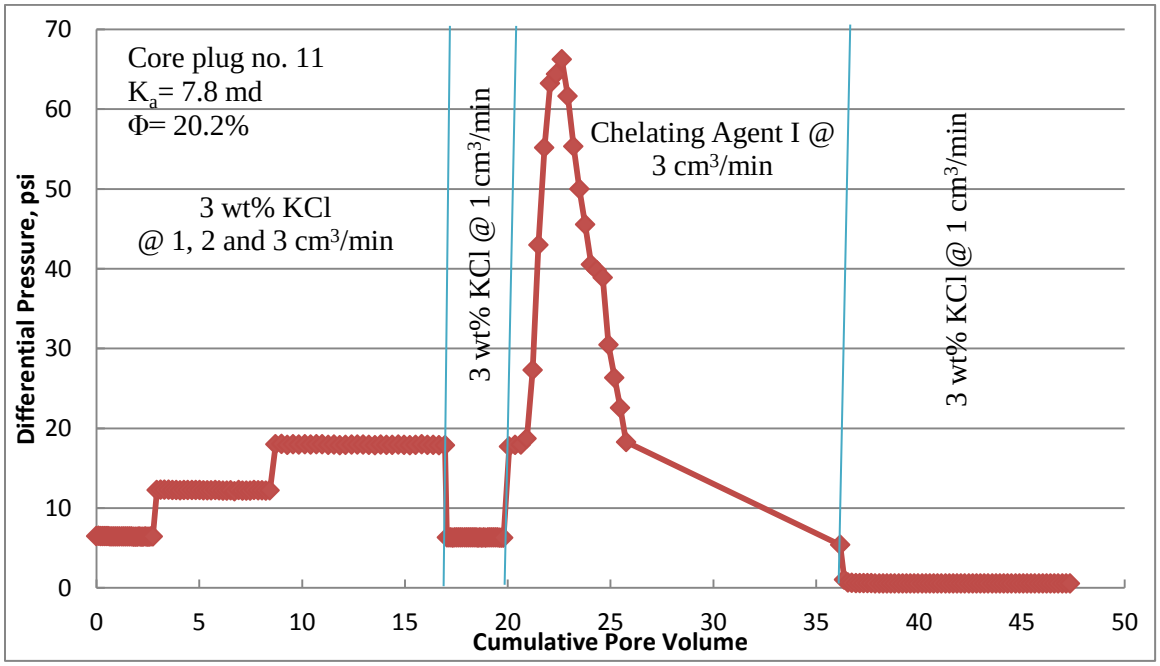

Figure 27 : Coreflooding performance of Chelating Agent I (pH 3-4, 3 cm^3/min, 200°F).

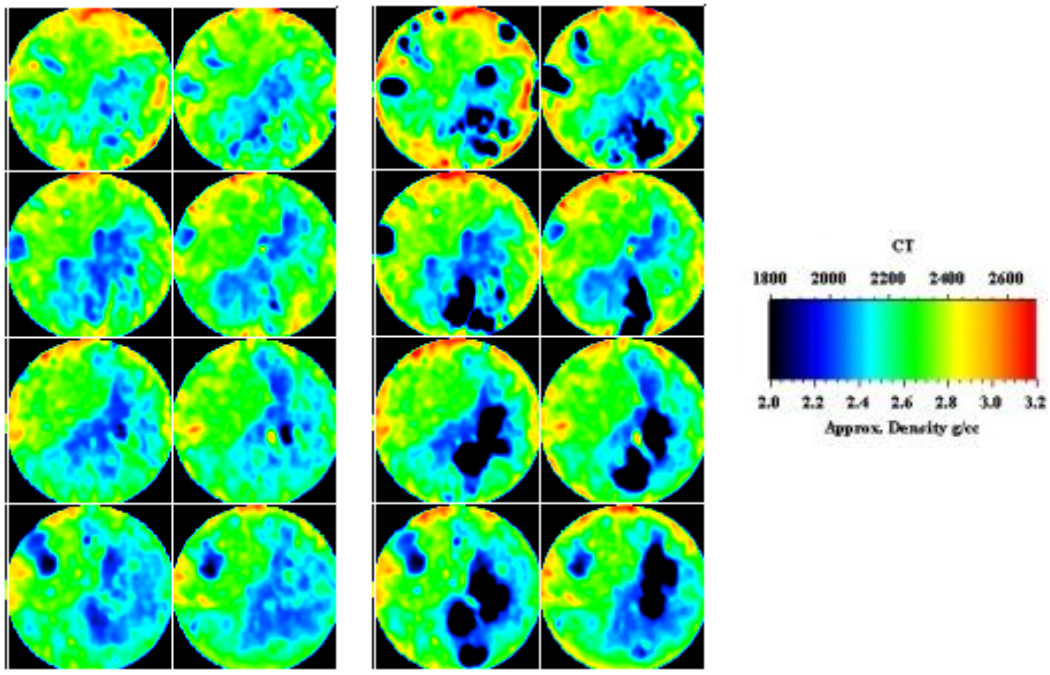

a) before acidizing b) after acidizing c) Density Scale

Figure 28: CT Scan images of core plug no. 11 (Chelating Agent I at 3.0 cm^3/min).

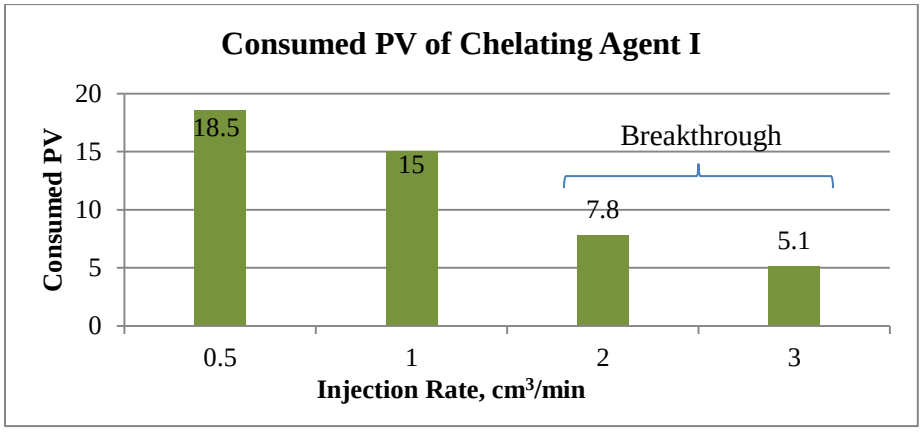

Figure 29: Effect of injection rate on coreflooding performance (Chelating Agent I).

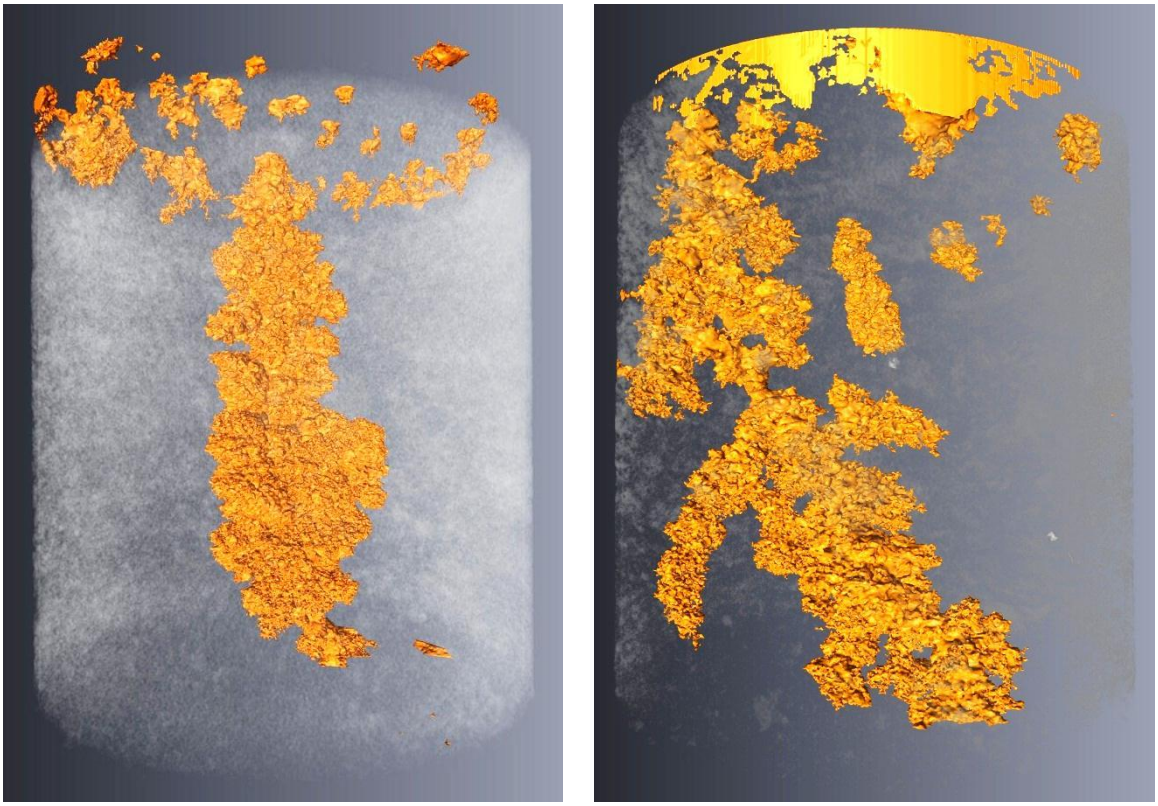

2.0 cm^3/min 3.0 cm^3/min

Figure 30: 3D visualizations of generated wormholes (Chelating Agent I).

4.1.1.4 Chelating Agent II

In addition to Chelating Agent I, Chelating Agent II was used at the injection rate which the first chelating agent did not succeed in accomplishing a breakthrough. Therefore, Chelating Agent II, initially has a pH value of >13, was injected at 1 cm^3/min through core plug sample no. 12. A breakthrough was observed after consuming 1.2 PV of Chelating Agent II, as seen in **Figure 31**. This PV_{BT} was comparable to that achieved by emulsified acid showed in Figure 10. The sudden drop in differential pressure can be related to the initial presence of small vugs inside the core plug sample, as seen in the CT scan images in **Figure 32**. The initial abundance of vugs in this core plug sample could explain the drop in pressure when brine was injected again at 1 cm^3/min. Initially, the differential pressure, when brine was injected at 1 cm^3/min, was 12-13 psi. However, when brine was injected again at 1 cm^3/min, after the step-rate test, the differential pressure was lowered to 10 psi. It is suspected that the high injection rates, 2 and 3 cm^3/min, have stimulated the sample mechanically by creating porethroats between large adjacent vugs with thin walls, and/or migrating some fine particles that were initially plugging porethroats.

This enhancement of permeability enabled Chelating Agent II to flow throughout the core plug sample without noticeable increase in differential pressure. Nevertheless, the dissolution of the core plug sample was very comparable to that of emulsified acid, and to the contrary of Chelating Agent I. In addition, the phenomenon of face dissolution was not observed, as shown in **Figure 33**, as in the cases of Chelating Agent I and 15 wt% HCl. The 3D visualization in **Figure 34** shows the generated wormhole throughout the core plug sample. With the use of micro-CT, a natural fracture was detected at the bottom

half of the core plug sample, as seen in Figure 34. This fracture enabled Chelating Agent I to flow easily and breakthrough with minimal require PV.

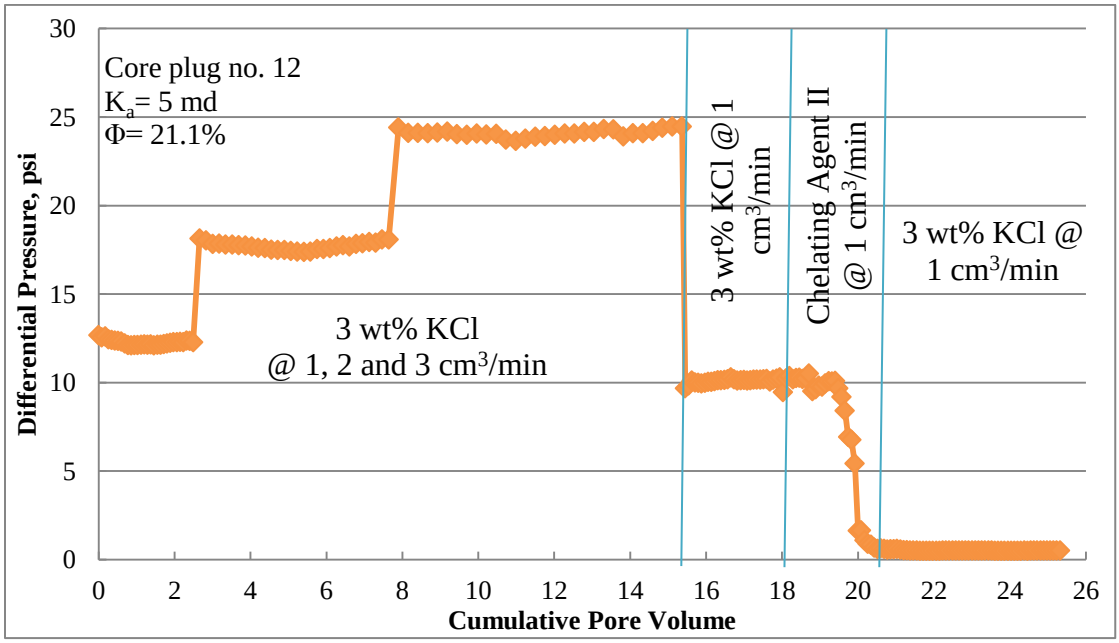

Figure 31: Coreflooding performance of Chelating Agent II (pH >13, 1 cm^3/min, 200°F).

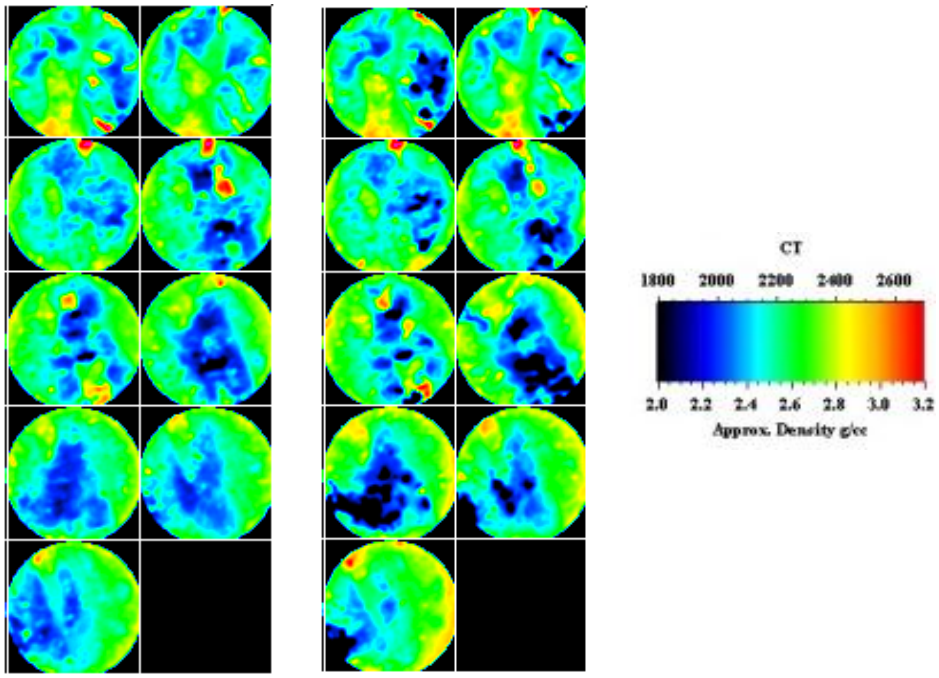

a) before acidizing b) after acidizing c) Density Scale

Figure 32: CT Scan images of core plug no. 12 (Chelating Agent II at 1.0 cm^3/min).

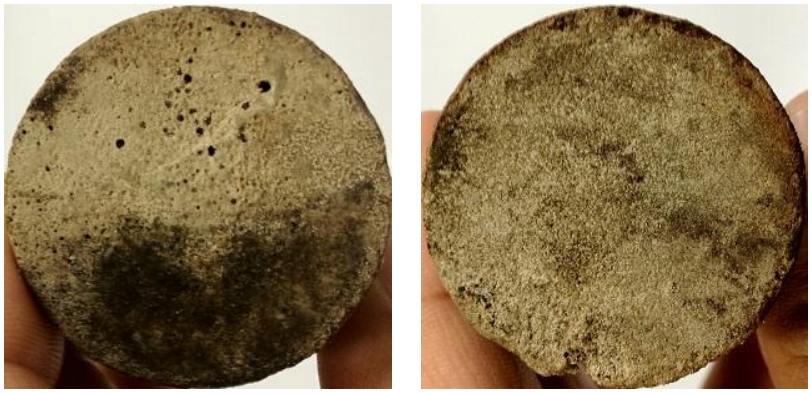

Inlet Outlet

Figure 33: Core plug no. 12 after injecting Chelating Agent II at 1.0 cm^3/min.

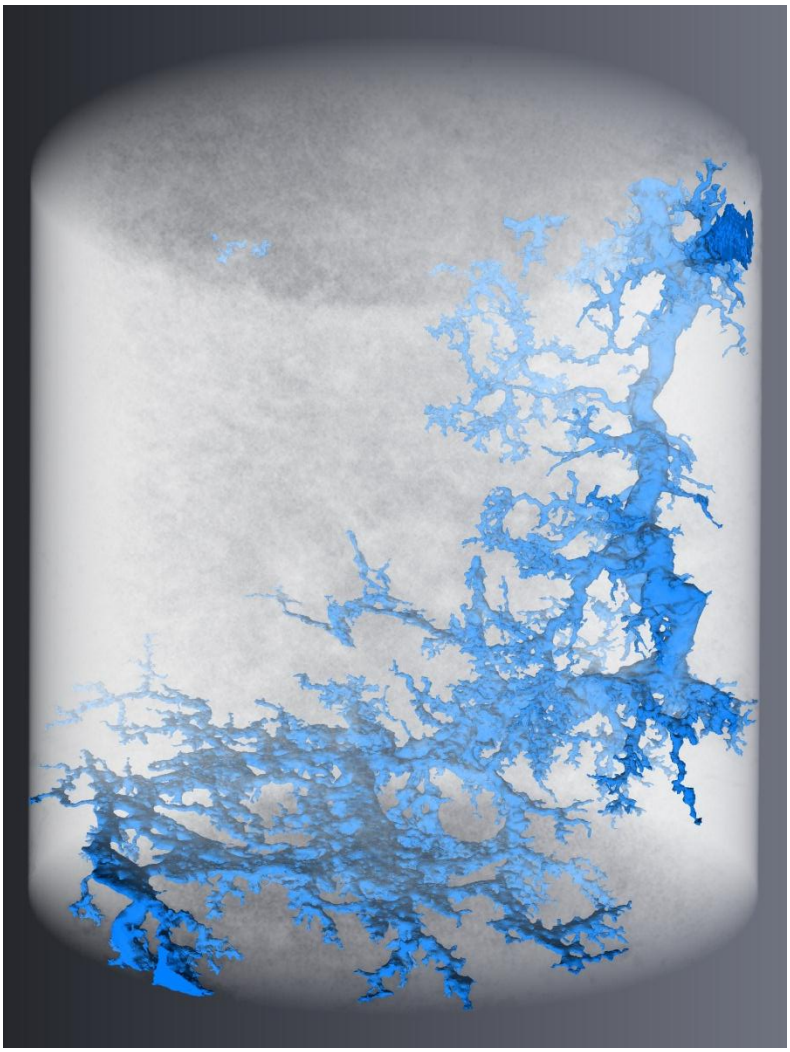

Figure 34: 3D visualizations of generated wormholes (Chelating Agent II, 1.0 cm^3/min).

4.1.2 Effect of Acid/Fluid Type

For this part of the study, core plug samples (25, 25B, 26 and 26B) from Indiana Limestone were used because of their high lithology consistency. As shown in Table 1, these samples have very similar petrophysical properties in terms of porosity and permeability. In addition, these samples have exactly the same percentage of calcite, as seen in Table 2. Therefore, this test should emphasize the effect of varying the stimulation fluid.

In all four experiments, the conditions were maintained exactly the same, while only varying the type of injected stimulation fluid. The conditions of these experiments are shown in **Table 5**. After analyzing the coreflooding pressure data, the performances of these four stimulation fluids are shown in **Figure 35** as a function of PV_{BT}. While HCl consumed 14.5 PV_{BT} using sample no. 2, it only consumed 4.9 PV_{BT} when sample no. 25 was used. The difference in lithology has impacted the performance of HCl especially in the presence of dolomite in sample no. 2. Emulsified acid, however, has consumed 0.5 PV_{BT} using sample no. 26B compared to 0.8 PV_{BT} using sample no. 4. The incremental decrease in PV_{BT} was not significant. Chelating Agent I showed significant improvement when sample no. 26 was used. The PV_{BT} was 2.5, while it did not achieve a breakthrough at 1 cm^3/min when samples no. 7, 8 or 9 were used. Chelating Agent II, on the contrary, has shown poor performance when sample no. 25B was used. It consumed 5.5 PV_{BT} compared to 1.2 PV_{BT} when sample no. 13 was used. The CT scan of used core plugs before and after the introduction of stimulation fluids are presented in **Figures 36-39**. Photos of inlet and outlet faces of the used core plug samples are presented in **Figure 40**. Although their PV_{BT} are close, HCl, in Figure 36, might show a very broad wormhole

compared to Chelating Agent II, in Figure 39. This was a result of the pushed dead volume of HCl through the sample, which increased the dissolution and broadened the wormhole. Chelating Agent II, on the other hand, was not as reactive as HCl, hence, the dissolution due to the dead volume was less.

The lithology has definitely affected the performance of Chelating Agent I and HCl. As for Chelating Agent II, the performance might have been affected; however, sample no. 13, through which Chelating Agent II performed well, had a facture that was not detected initially. This might have improved its performance in the first place.

Table 5: Coreflooding experiments conditions and results to determine the effect of injected fluid*.

	Stimulation Fluid	Core plug no.	Injection Rate cm^3/min	pH	Breakthrough PV
1	15% HCl	25	1	0	4.93
2	Emulsified Acid (15% HCl)	26B	1	0	0.51
3	Chelating Agent I (20 wt%)	26	1	3-4	2.47
4	Chelating Agent II (20 wt%)	25B	1	13	5.54

* All experiments were conducted at 200˚F, 1,500 psi of confining pressure, and 1,000 psi of back pressure.

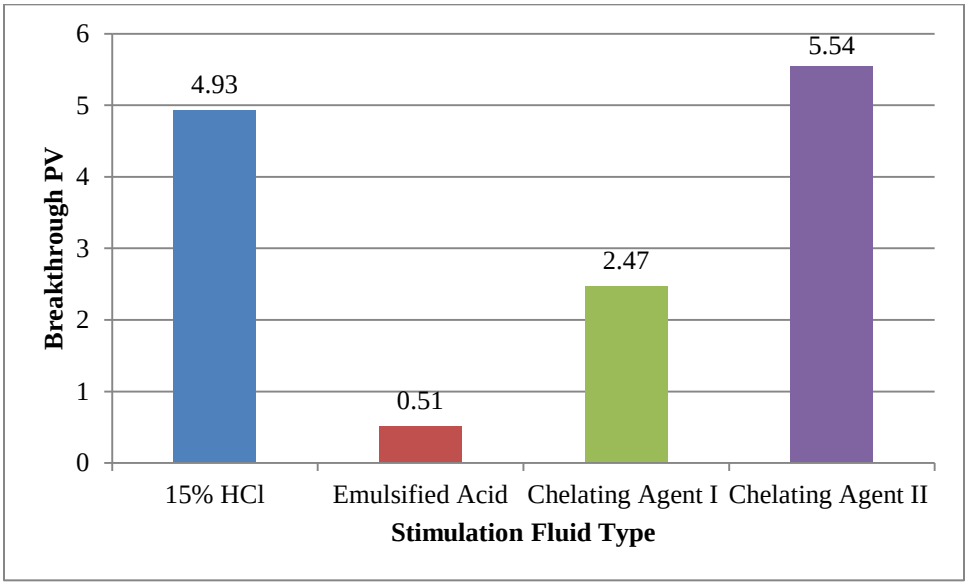

Figure 35: Effect of stimulation fluid type on PV_{BT} using Indiana limestone samples.

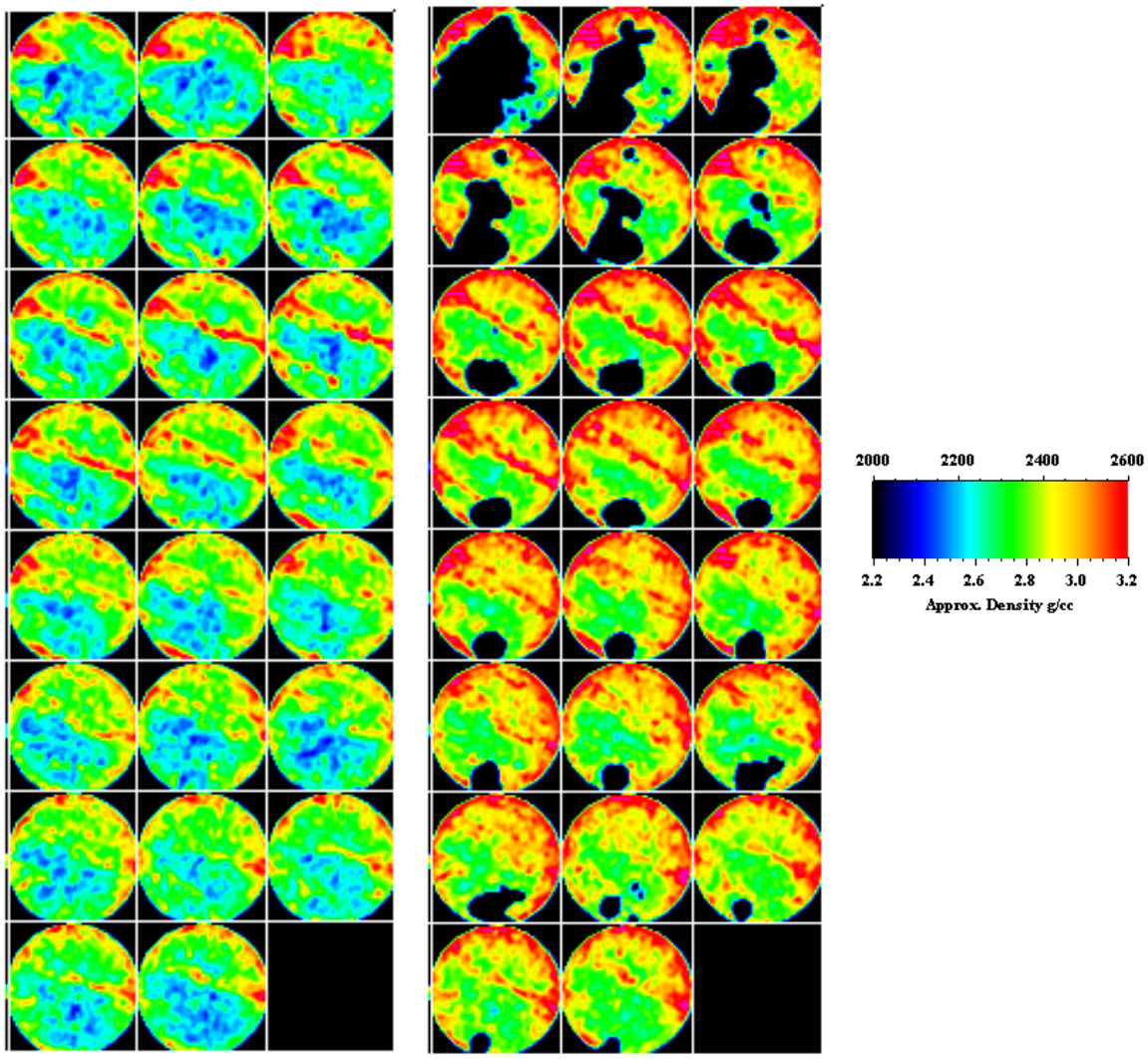

a) before acidizing b) after acidizing c) Density Scale

Figure 36: CT Scan analysis of core plug no. 25 (15 wt.% HCl at 1.0 cm^3/min).

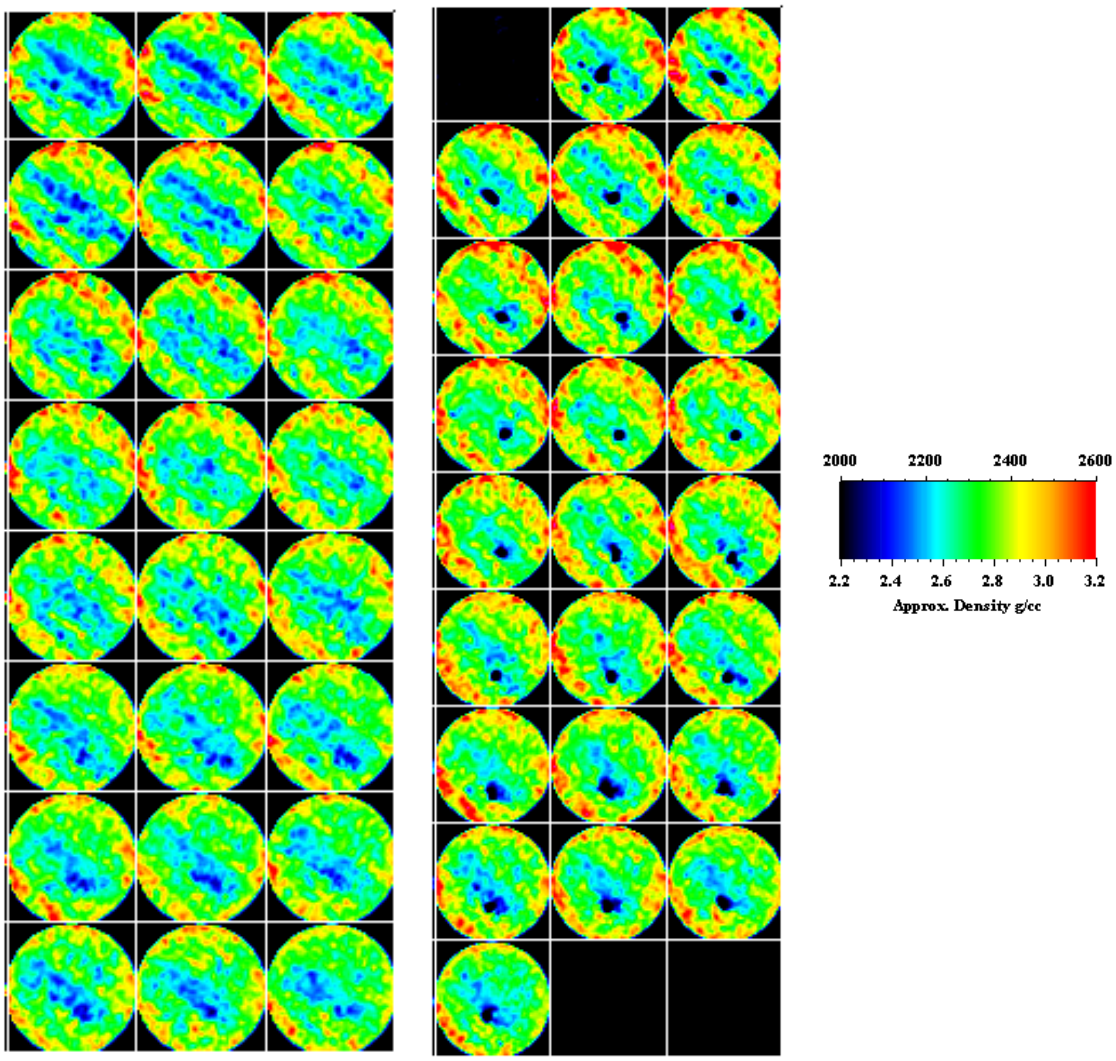

a) before acidizing b) after acidizing c) Density Scale

Figure 37: CT Scan analysis of core plug no. 26B (Emulsified acid at 1.0 cm^3/min).

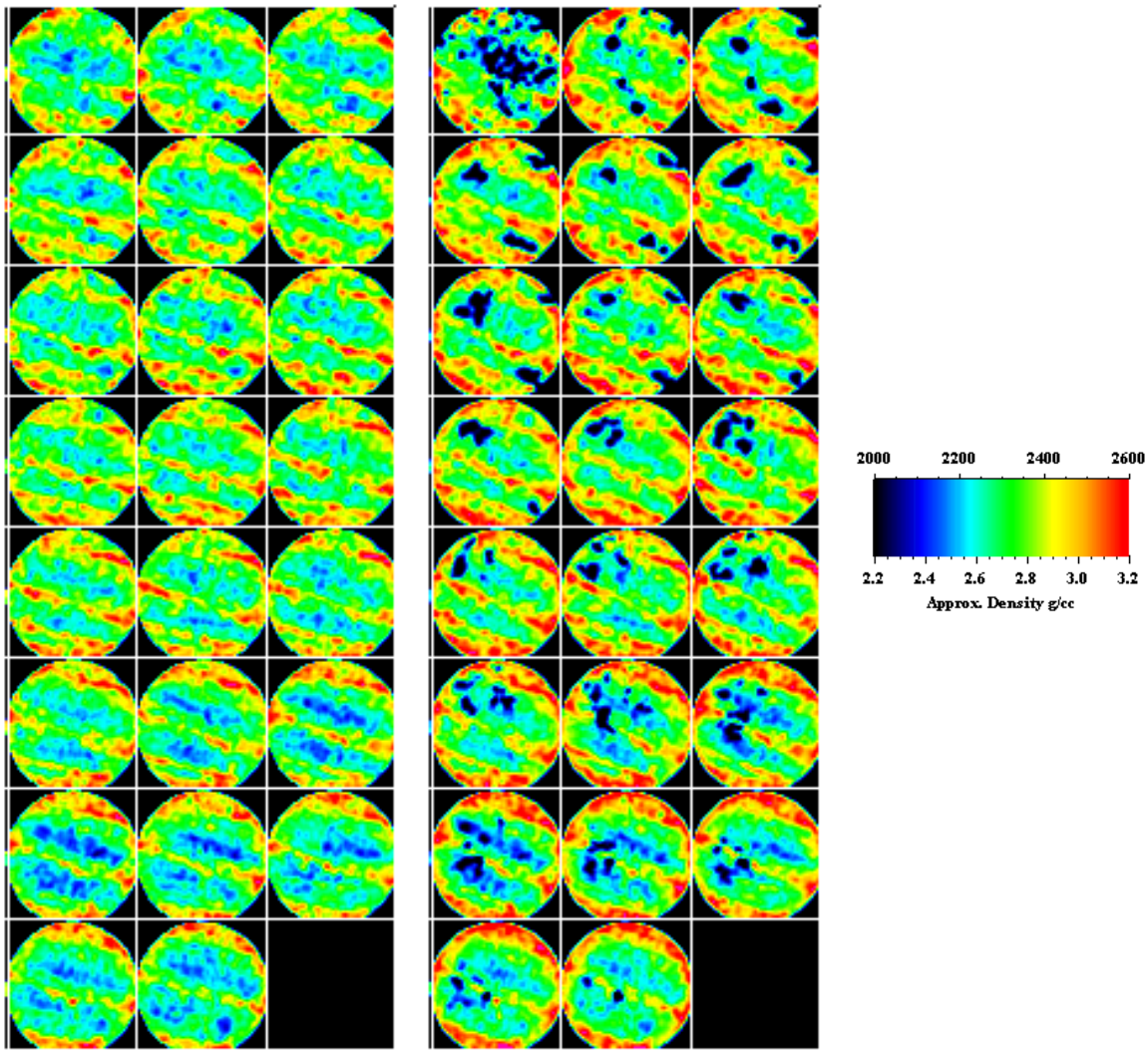

a) before acidizing b) after acidizing c) Density Scale

Figure 38: CT Scan analysis of core plug no. 26 (Chelating Agent I at 1.0 cm^3/min).

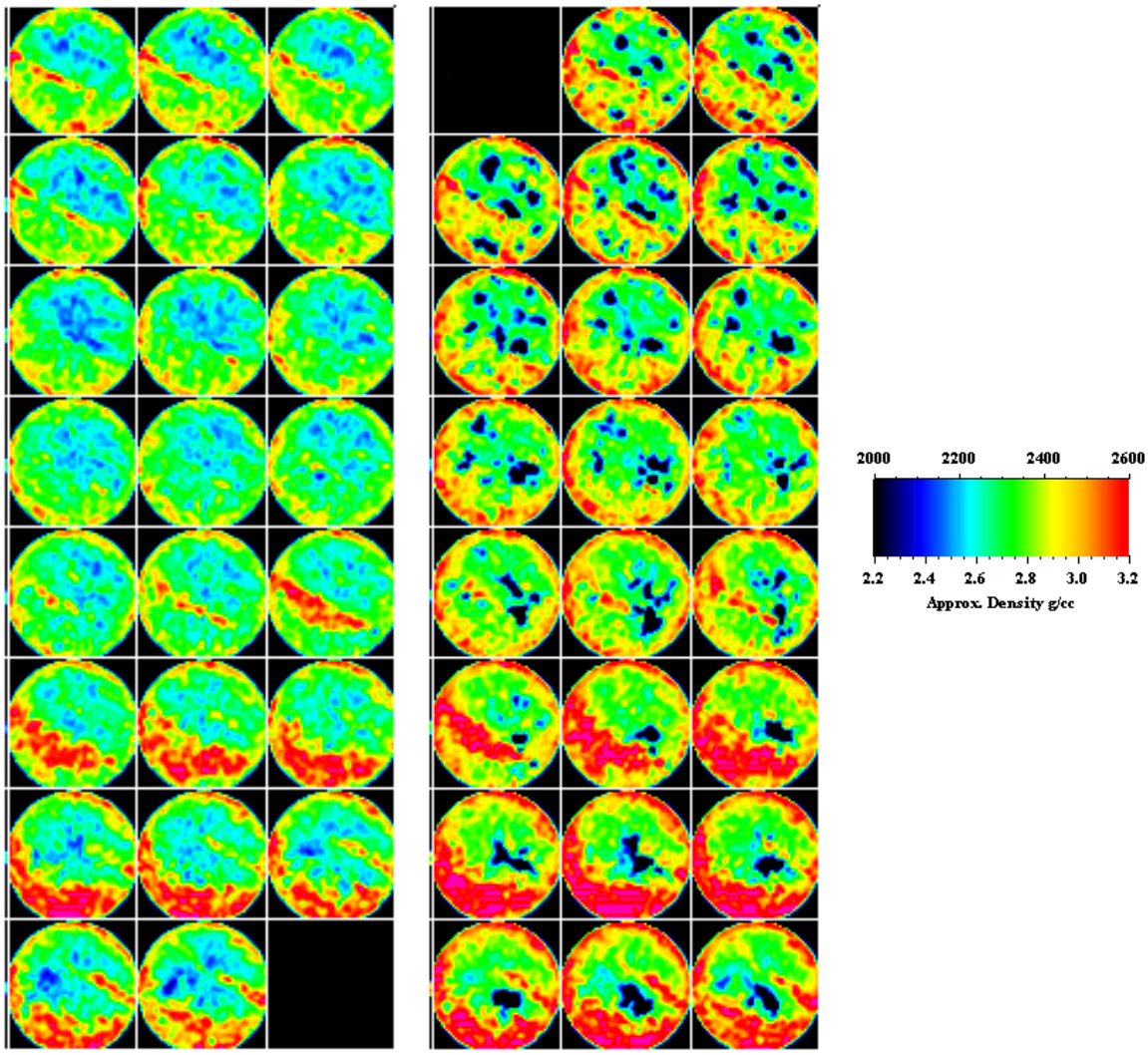

a) before acidizing b) after acidizing c) Density Scale

Figure 39: CT Scan analysis of core plug no. 25B (Chelating Agent II at 1.0 cm^3/min).

Stimulation Fluid (Sample no.)	Inlet	Outlet
15 wt.% HCl (25)		
Emulsified acid (26B)		
Chelating Agent I (26)		
Chelating Agent II (25B)		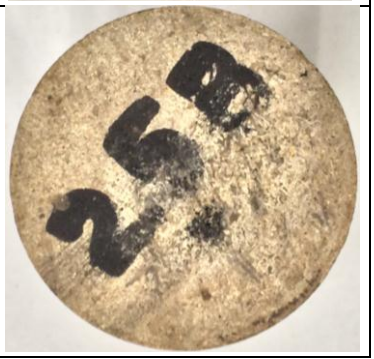

Figure 40: Core plugs no. 25, 26B, 26 and 25B after injecting different stimulation fluids.

4.1.3 Effect of pH on Chelating Agents

The pH value of Chelating Agents I and II were varied to examine the influence of pH on the chelation mechanism. Since initially Chelating Agent I had a pH value of 3-4m sodium hydroxide (NaOH) was added to raise the pH to almost 13. On the contrary, Chelating Agent II had a pH value of more than 13; therefore, it was lowered to 3.5 by adding HCl. The coreflooding performances of both pH-altered chelating agents are shown in **Figures 41 and 42**.

When injected at 1 cm^3/min, high-pH Chelating Agent I performed slightly better than its low-pH version by achieving 4.1 PV_{BT} rather than 5.1 PV_{BT} at 3 cm^3/min injection rate. The differential pressure behaved differently compared to the raw Chelating Agent I experiments. In Figure 41, the differential pressure increased and dropped gradually, where it formally increased dramatically and declined slowly, as seen in Figures 25 and 27. However, this result was not conclusive as the core plug sample was broken through from the side, as seen in **Figure 43**, which might have lowered the PV_{BT}. Nonetheless, the consumed PV_{BT} is still very high compared to that achieved by Chelating Agent II or emulsified acid. In addition, the associated dissolved material was not observed when this pH-modified version of Chelating Agent I was used.

The low-pH version of Chelating Agent II (pH 3.5) achieved a breakthrough after consuming 8.1 PV at an injection rate of 1 cm^3/min, as seen in Figure 42. Formally, Chelating Agent II (pH 13) achieved a breakthrough after consuming 1.2 PV. The mechanism of dissolution, hence the differential pressure behavior, has changed according to the new pH value, which was a major influence on both chelating agents.

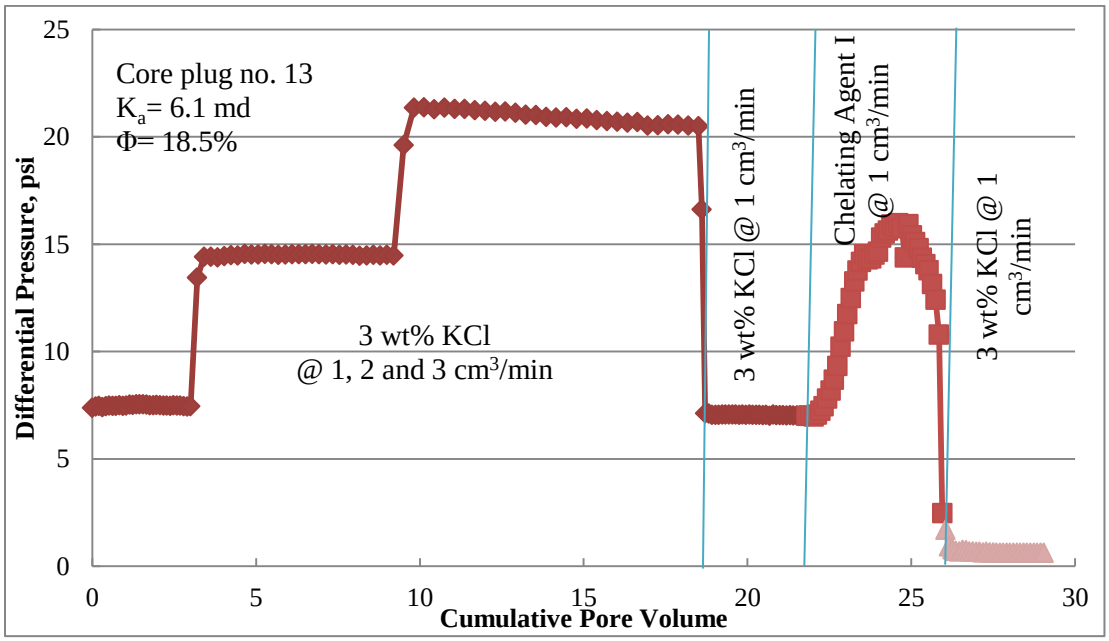

Figure 41: Coreflooding performance of Chelating Agent I (pH 13, 1 cm^3/min, 200°F).

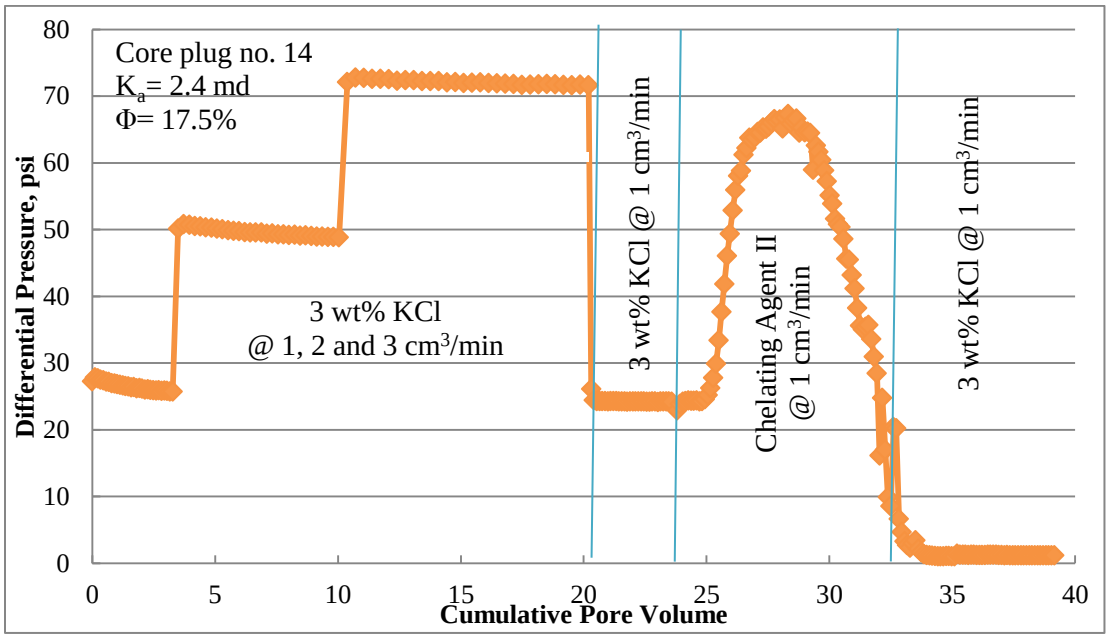

Figure 42: Coreflooding performance of Chelating Agent II (pH 3.5, 1 cm^3/min, 200°F).

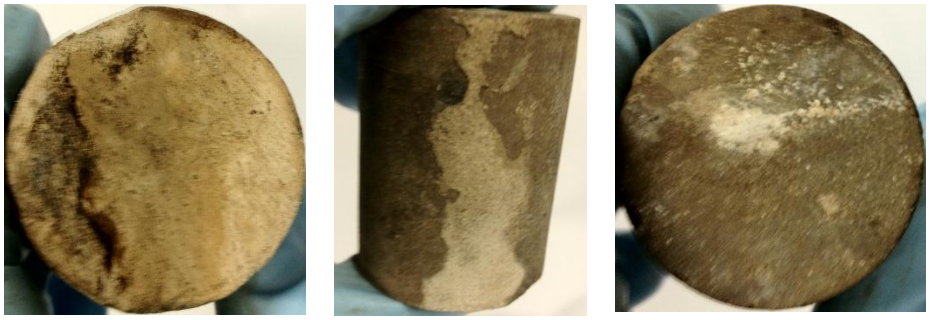

Inlet Side breakthrough Outlet

Figure 43: Core plug no. 13 after injecting Chelating Agent I (pH 13, 1.0 cm^3/min).

4.2 Results of NMR Characterization of Formed Wormholes

The NMR analysis was focused on six cases which included the use of emulsified acid, Chelating Agent I and Chelating Agent II at different injection rates.

4.2.1 Emulsified Acid at 0.5 cm^3/min

The 5MHz CPMG chart, **Figure 44** shows that in the pre-stage (blue line) most of the detected porosity was initially macro-pores (20-2000 milliseconds) with very minimal micro-pores presence (2-20 milliseconds). This indicated that either micro-pores barely existed initially, or the porethroats of micro-pores were mostly sealed which resulted in preventing the brine from saturating them. Nonetheless, the system originally can be referred to as a single pore system (macro-pores).

After the introduction of acid, the sample was analyzed. The post-stage (red line) shows a dramatic change in the pores distribution. The macro-pores, which previously dominated the detected porosity, merged with the wormhole porosity, which at this stage was not detected due to the in ability to sustain the saturation fluid inside the wormhole porosity. The micro-pores appeared differently in two distinctive sizes represented by two peaks (0.06-7 milliseconds and 10-600 milliseconds). The acid was able to enlarge some of the micro-pores and connect others, therefore, creating two species of micro-pores. The interconnectivity (diffusion coupling) between these two species is very high as seen in Figure 44.

When the Teflon tube was used, the wormhole porosity was detected (300-3000 milliseconds), as the green line shows in Figure 44. The use of Teflon tube maintained the core plug sample in full saturation which enabled the NMR to detect the new

porosity. As seen in Figure 44, three peaks are present which suggested that the pore system has become triple rather than dual. The first two peaks represent micro- (0.1-10 milliseconds) and meso-pores (10-200 milliseconds), while the third peak represents the macro-pores (300-3000 milliseconds), which merged with the wormhole. Moreover, the acid was able to keep the whole detected pore system connected by increasing the interconnectivity (diffusion coupling).

Furthermore, the wormhole porosity peak (300-3000 milliseconds) ends shortly after the original porosity (20-2000 milliseconds). This indicates that the acid did not dramatically increase the porosity, yet was able to significantly connect the three pore systems to each other.

The decrease in intensities of peaks between the three analyses can be traced back to the presence of hydrocarbons inside the pores (originated from the emulsified acid). Although the sample was flushed with brine after the breakthrough, some of the pores might still be partially filled with diesel, which prevented the core plug sample from reaching a full saturation level even while utilizing the Teflon tube.

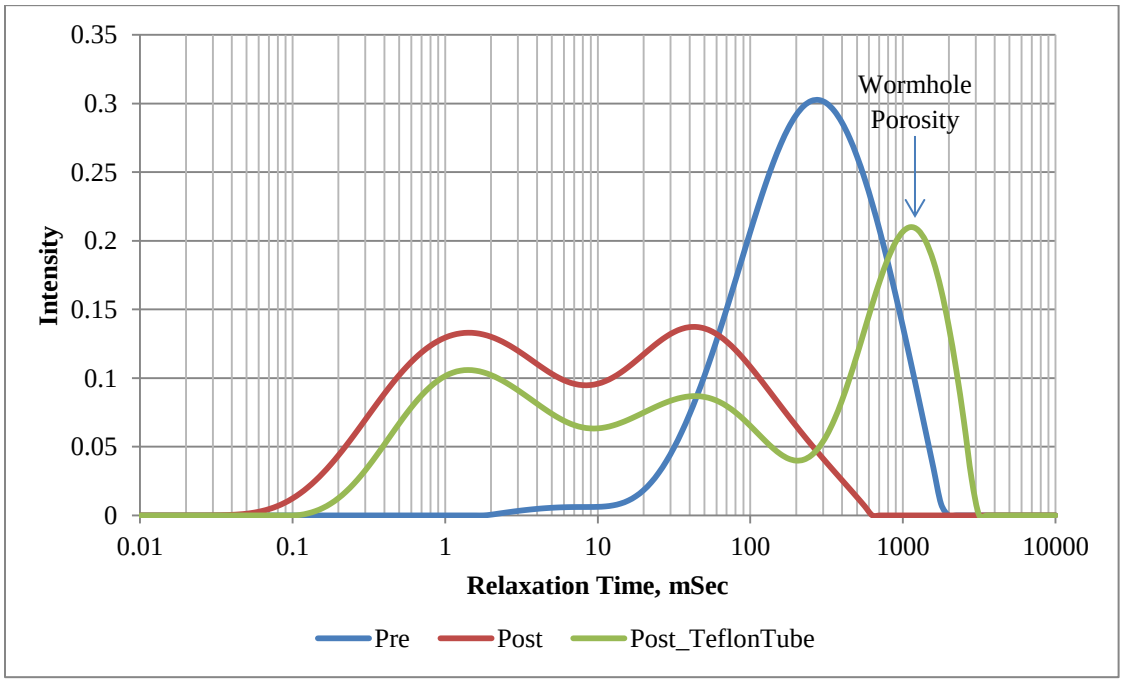

Figure 44: 5MHz CPMG chart of core plug no. 3 (Emulsified Acid at 0.5 cm^3/min).

4.2.2 Emulsified Acid at 2.0 cm^3/min

The 5MHz CPMG analysis, **Figure 45**, shows that micro-pores (3-30 milliseconds) and macro-pores (30-5000 milliseconds) initially existed with high interconnectivity. Micro-pores were minimal compared to macro-pores due to isolation. Although it might appear as a single-pore system due to the high diffusion coupling, the micro-pores peak is very distinctive from the macro-pores, which suggests that it is initially a single-pore system.

The post-acidizing analysis shows an increase in the intensity of the macro-pores (20-800 milliseconds) due to dissolving some of the micro-pores and enlarging some of the macro-pores. In addition, the micro-pores slightly increased (2-10 milliseconds) indicating that the acid has re-connected some of the initially isolated pores. However, the increase in micro-pores is not comparable to that observed in the previous test, Figure 44. This can be an effect of the high injection rate used in this experiment. The wormhole porosity was not detected at this stage due to the in inability to sustain the saturation fluid inside the created wormhole.

After using the Teflon tube, the wormhole porosity was detected as an extension of the macro-pores (30-3000 milliseconds). Previously, the peak of macro-pores ended at 800 milliseconds. When the core plug was fully saturated, the wormhole appeared by extending the peak of macro-pores to 3000 milliseconds, which indicates that this acid has not increased the porosity dramatically, yet maintained and partially increased the interconnectivity between the pore systems.

The intensity of each peak has slightly dropped as a result of the diesel residual in the pores. This hydrocarbon phase can fill some of the pores and/or alter the wettability.

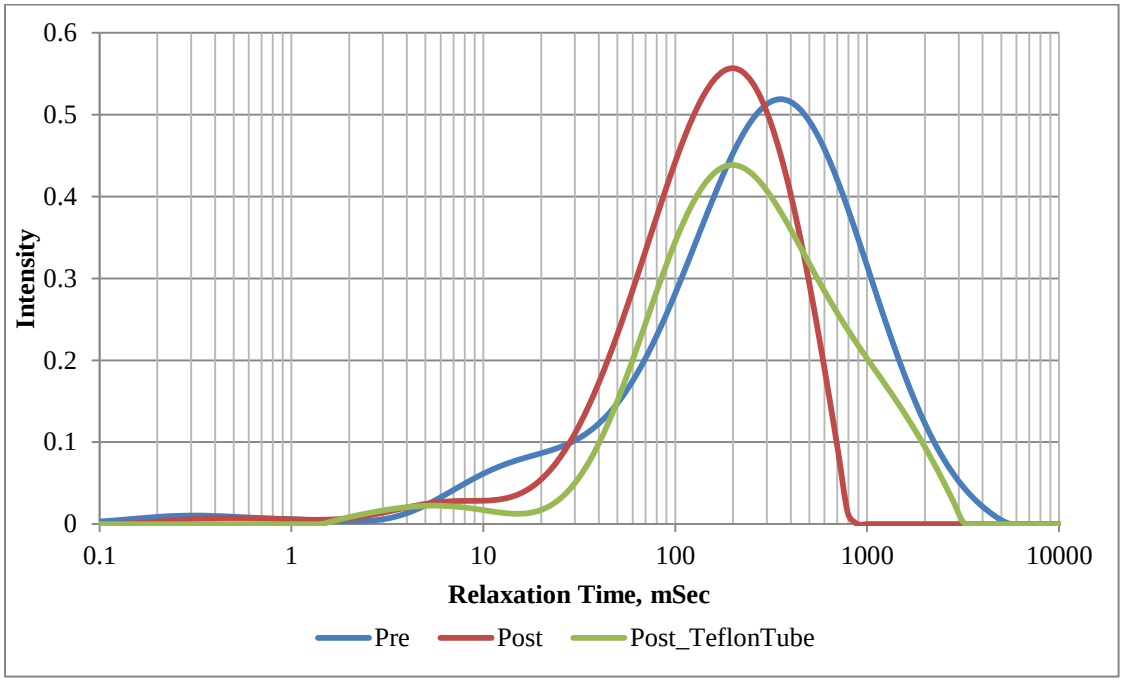

Figure 45: 5MHz CPMG chart of core plug no. 5 (Emulsified Acid at 2.0 cm^3/min).

4.2.3 Chelating Agent I at 0.5 cm^3/min

The 5MHz CPMG chart in **Figure 46** shows that the system was initially a dual-pore system where the micro-pores resided between 4-30 milliseconds, and macro-pores resided between 30-1000 milliseconds. In addition, the two pore systems were initially connected with a relatively low diffusion coupling.

When the stimulation fluid was injected through the core plug sample, the pore system changed dramatically. The post-stage in Figure 46 shows a sharp increase in the macro-pores (50-700 milliseconds), while micro-pores (2-5 milliseconds) were further reduced and isolated. The diffusion coupling has decreased between the two pore systems. The porosity of the created dissolution was not detected at this stage due to the inability to sustain saturation fluid in the big vugs, as seen in Figure 18.

When Teflon tube was used, the large vugs were able to sustain the saturation fluid. As seen in Figure 46, the post-acidizing stage with Teflon tube shows a new peak between 700-4000 milliseconds. This peak is associated with the large vugs created at the inlet face of the core plug sample, as seen in Figures 17 and 18. The huge range of relaxation time, which this peak resides on, indicates an extreme change in the porosity of the core plug. Although Chelating Agent I was not able to create a breakthrough in this sample, it managed to increase the porosity by dissolving large volumes of the rock, as seen in Figure 19. The diffusion coupling was decreased between the micro- and macro-pores, however, the macro-pores were well-connected to the large vugs.

The intensity of the peaks decreased post stage and the Teflon tube stage due to precipitating Chelating Agent I with time. The core plug sample was not fully saturated

because this precipitation plugged the porethroats connection part of the pores, which prevented the saturation fluid from reaching them.

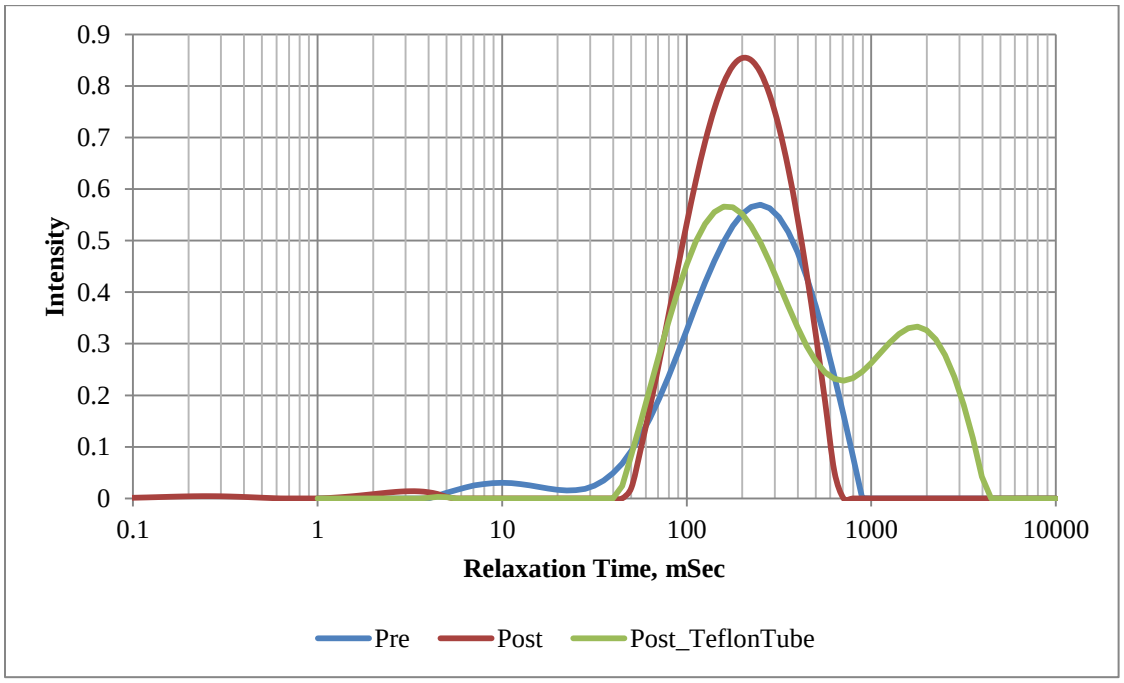

Figure 46: 5MHz CPMG chart of core plug no. 6 (Chelating Agent I, pH 3-4, 0.5 cm^3/min).

4.2.4 Chelating Agent I at 1.0 cm^3/min

Initially, the 5MHz CPMG chart in **Figure 47** show that prior to introducing Chelating Agent I to the sample, macro-pores (30-1000 milliseconds) dominated the porosity with low presence of micro-pores (3-30 milliseconds). In addition, the dual-pore system had a relatively high diffusion coupling between detected pore systems.

When Chelating Agent I was injected, the peak of macro-pores slightly was increased in intensity (20-800 milliseconds), while the micro-pores (3-10 milliseconds) were reduced and isolated from macro-pores, which decreased the interconnectivity between the two pore systems. The porosity associated with the large dissolution at the inlet face of the core plug sample, Figure 22 (a), was not detected at this stage due to the inability to sustain the saturation fluid inside the dissolved area.

By using the Teflon tube, the porosity associated with the dissolved part of the inlet face was detected, as seen in Figure 47 (700-2000 milliseconds). This peak should not be mistaken with a wormhole peak even though it resembles the same characteristics. The core plug samples in this experiment lost around 15 vol.% as deposited material, as seen in Figure 22 (b). Therefore, the porosity associated with this lost part was not accounted for during the NMR analysis. Nonetheless, this porosity would have appeared as a large peak at much larger relaxation time, with similar characteristics to the peak in Figure 46 (700-4000 milliseconds). The diffusion coupling decreased as the micro-pores were isolating the micro-pores because of plugging the porethroats with the deposited material.

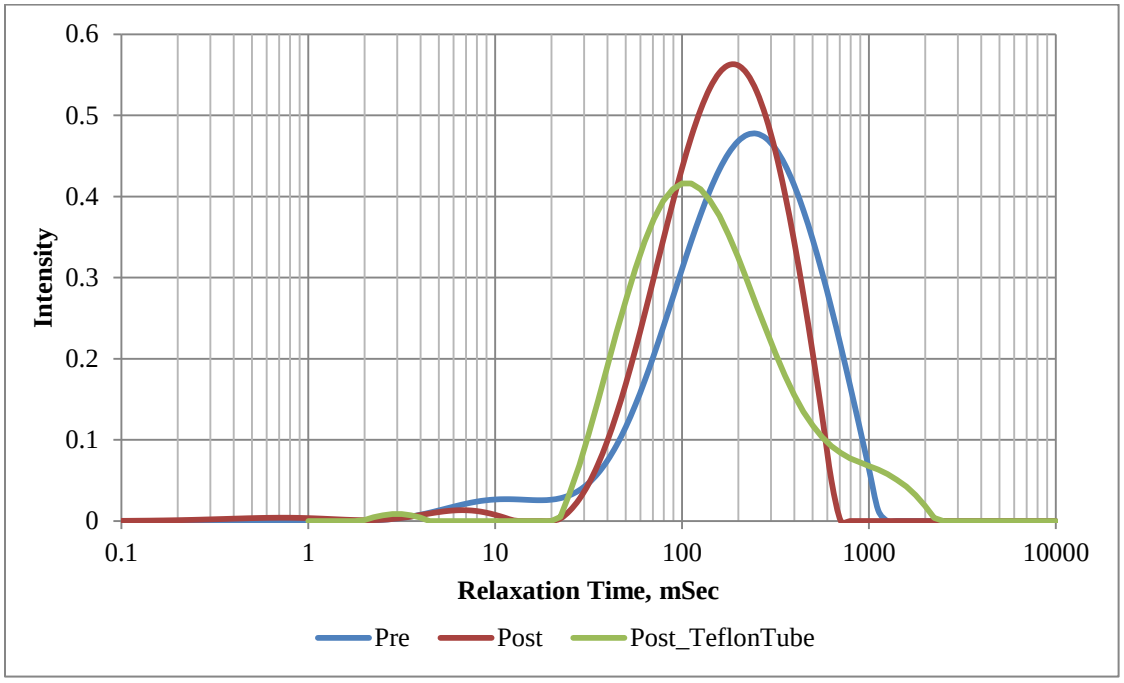

Figure 47: 5MHz CPMG chart of core plug no. 7 (Chelating Agent I, pH 3-4, 1.0 cm^3/min).

4.2.5 Chelating Agent I at 2.0 cm^3/min

The 5MHz CPMG chart in **Figure 48** shows that the system had initially macro-pores (30-800 milliseconds) constituting the majority of the detected porosity, while micro-pores (3-20 milliseconds) were hardly detected due to natural obstructions. The diffusion coupling was very low since the macro- and micro-pores were barely connected. By looking at the blue line in Figure 48, the system can be recognized as a dual-pore system.

After injecting Chelating Agent I, the initial diffusion coupling was further reduced, and the micro-pores (1-6 milliseconds) were further isolated due to plugging porethroats with the particles carried by the spent fluid. The macro-pores (30-700 milliseconds) significantly increased by enlarging some of the micro-pores. Still, the wormhole porosity was not detected at this stage due to the inability to sustain the saturation fluid inside the wormhole.

When Teflon tube was used to maintain the sample saturated, the peak of macro-pores extended to higher relaxation time (50-2000 milliseconds). This extension is associated with wormhole porosity. The wormhole was well connected to the macro-pores since they constituted most of its porosity. Micro-pores (2-5 milliseconds) were isolated as seen earlier. The injection of Chelating Agent I has increased the porosity significantly while sealing the connecting channels between different pore sizes. The pore system after the introduction of Chelating Agent I can be referred to as a single-pore system.

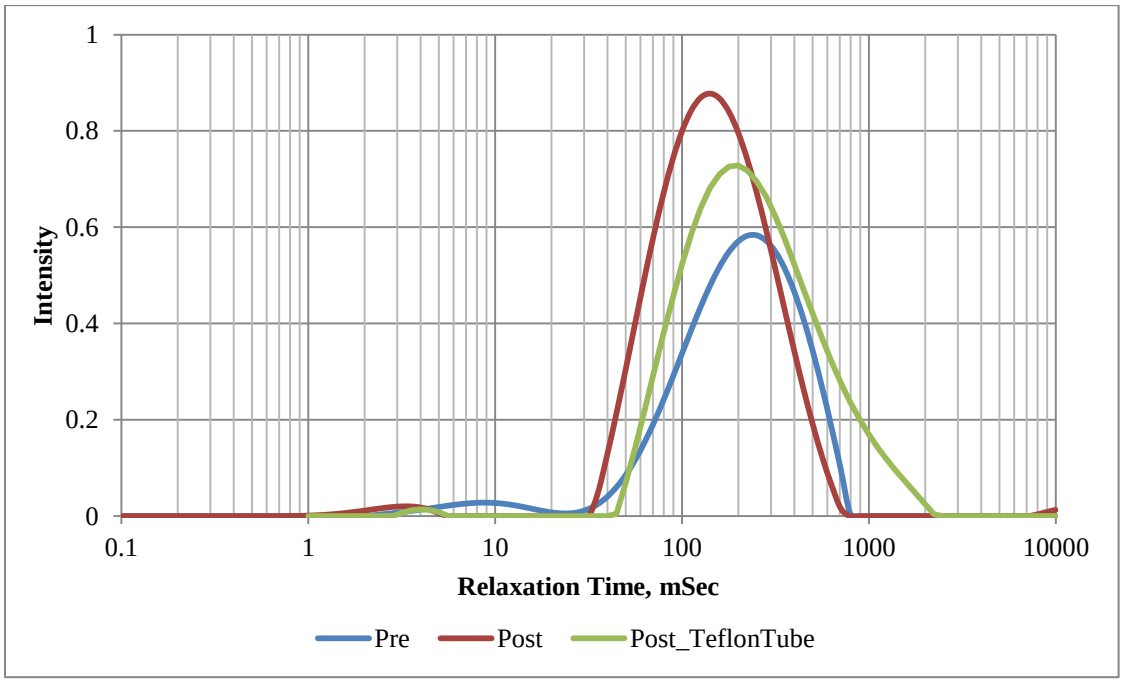

Figure 48: 5 MHz CPMG chart of core plug no. 10 (Chelating Agent I, pH 3-4, 2.0 cm^3/min).

4.2.6 Chelating Agent II at 1.0 cm^3/min

The 5MHz CPMG chart in **Figure 49** shows that, originally, the system consisted of a major peak representing macro-pores (30-800 milliseconds) and a minor peak representing micro-pores (2-10 milliseconds). The pore system can be referred to as a single-pore system due to the absence of sufficient micro-pores population, which can be sealed naturally and couldn't not be saturated and detected. In addition, there was no interconnectivity (diffusion coupling) between the macro-pores and micro-pores initially.

Chelating Agent II was able to disturb the initial pore system by increasing the micro-pores significantly (0.1-10 milliseconds), and connect them with macro-pores (0.1-2500 milliseconds). The new peaks are a result of dissolving barriers isolating micro-pores, enlarging micro-pores and connecting them with macro-pores. Initial macro-pores decreased as a result of merging with the wormhole porosity, which was not detected at this stage, as a result to the inability to sustain saturation fluid inside the wormhole. The diffusion coupling has increased dramatically, indicating the pre-existence of sealed (isolated) micro-pores in the system. At this stage, the system can be referred to as a dual-pore system.

After using the Teflon tube, a new peak representing the wormhole porosity was detected (400-2000 milliseconds). This peak was very similar to that created by emulsified acid at Figure 44. The diffusion coupling between the triple-pore systems was relatively decreased due to precipitation with time, which resulted in plugging some of the pores and porethroates. Nonetheless, the three different pore sizes can be considered well-connected.

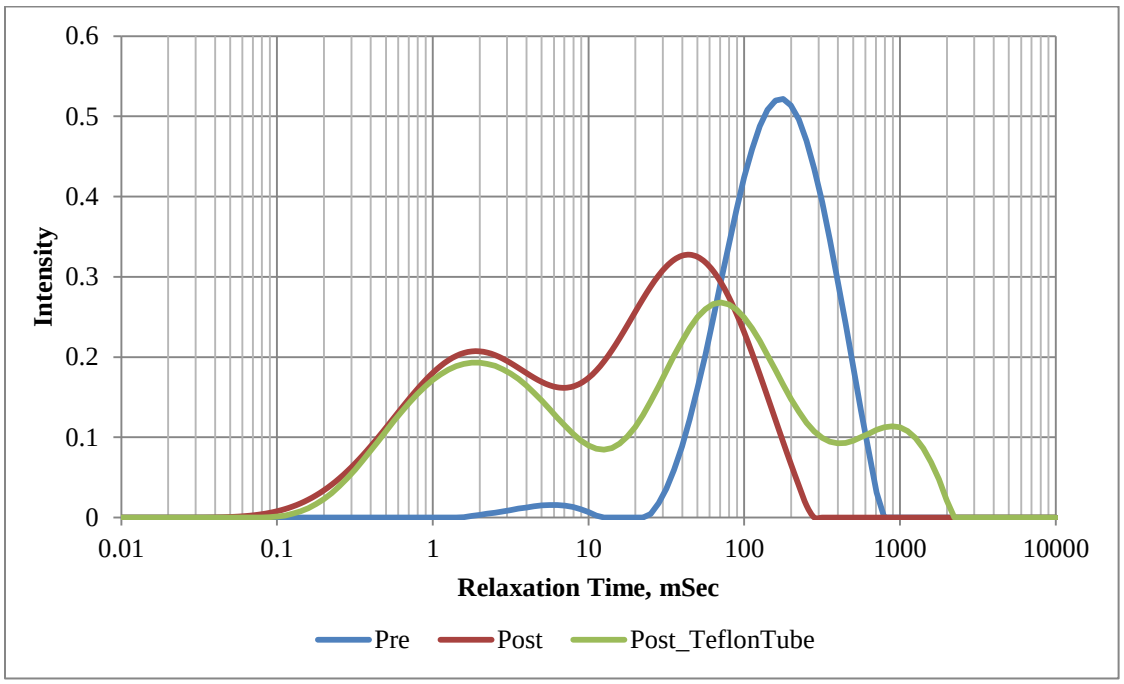

Figure 49: 5MHz CPMG of core plug no. 13 (Chelating Agent II, pH>13, 1 cm^3/min).

5 CHAPTER 5

CONCLUSIONS

The importance of wormhole characterization originates from its vital role in the evaluation and design of acid stimulation treatments. Typically, the characterization of wormholes is done using the coreflooding differential pressure data and CT scan analysis technique. In this work, NMR has been introduced and evaluated as an additional characterization technique for wormholing. By using different acids, the resulting wormholes were variant and unique, consequently, providing better opportunities to validate the NMR technique. Based on the results and findings of this study, the followings were concluded:

1- Nuclear Magnetic Resonance (NMR) introduced accurate analysis, in terms of pore size distribution, to different characteristics of the wormholing process of an acid.
2- Coreflooding differential pressure data and CT scan analysis provided verification of breakthrough occurrence, and suggested qualitatively the size and path of a wormhole.
3- NMR, as a wormholing characterizing tool, indicated the changes in porosity and pore-size distribution, and the diffusion coupling of different pore systems.
4- Complete core plug saturation by using a Teflon tube has significantly enhanced the NMR detection.
5- NMR was able to detect the materialization of formation damage inside samples.

6- NMR analysis was consistent with and complementing the CT scan analysis.

7- Using samples from Formation X, at an injection rate of 0.5 cm^3/min, only emulsified acid achieved a breakthrough. At an injection rate of 1 cm^3/min, emulsified acid, 15 wt% HCl, and Chelating Agent II achieved breakthrough. Chelating Agent I only achieved a breakthrough when injected at 2 and 3 cm^3/min.

8- Face dissolution was observed when Chelating Agent I and 15 wt% HCl were used at 0.5 and 1 cm^3/min.

9- Increasing the injection rate enhanced the performance of 15 wt% HCl and Chelating Agent I. The performance of emulsified acid was not enhanced when the injection rate was increased.

10- Chelating Agents I and II are pH-dependent.

11- Chelating Agent I produced a mud-like material, which was identified as calcite and dolomite.

12- Using samples from Indiana limestone, emulsified acid achieved 1.1 PV_{BT}, Chelating Agent I achieved 2.7 PV_{BT}, 15 wt% HCl achieved 5.9 PV_{BT}, and Chelating Agent II achieved 6.2 PV_{BT}.

13- Lithology heterogeneity only affected the performances of HCl and Chelating Agents I and II.

14- NMR analysis showed a sharp decrease in the interconnectivity between micro- and macro-porosities when Chelating Agent I was used. Emulsified acid and Chelating Agent II showed an increase in the interconnectivities between the two porosities.

References

[1] Akkurt, R., Kersey, D. and Zainalabedin, K. "Towards Everyday-NMR: an Operator's Perspective," *Petrophysics*, **50**(6), December 2009, pp. 495-510.

[2] Al-Mutairi, S.H. Al-Obied, M.A., Al-Yami, I.S., Shebatalhamd, A.M., and Al-Shehri, D.A., 2012. "Wormhole Propagation in Tar During Matrix Acidizing of Carbonate Formation," SPE 151560 paper presented at the International Symposium and Exhibition on Formation Damage Control, Lafayette, Louisiana, USA, 15-17 February.

[3] Al-Mutairi, S.H., Nasr-El-Din, H.A., and Hill, A.D. 2009. "Droplet Size Analysis of Emulsified Acid," SPE 126155 paper presented in the SPE Saudi Arabia Section Technical Symposium and Exhibition, al-Khobar, Saudi Arabia, 9-11 May.

[4] Buijse, M.A. 1997. "Mechanisms of Wormholing in Carbonate Acidizing," SPE 37283 paper presented at the SPE International Symposium on Oilfield Chemistry, Houston (TX), USA, 18-21 February.

[5] Buijse, M.A. and van Domelen, M.S. 1998. "Novel Application of Emulsified Acids to Matrix Stimulation of Heterogeneous Formations," SPE 39583 paper presented at the SPE International Symposium on Formation Damage Control, Lafayette, Louisiana, USA, 18-19 February.

[6] Doughty, D.A. and Maerefat, N.L. "Preliminary Transformation of an NMR Spectrometer into an NMR Imager for Evaluating Fluid Content and Rock Properties of Core Samples," *The Log Analyst*, March-April 1989, pp. 78-84.

[7] Eldestein, W.A., Vinegar, H.J, Tutunjian, P.N., Roemer, P.B., and Mueller, O.M. 1988. "NMR Imaging for Core Analysis," SPE 18272 paper presented at the 63rd Annual Technical Conference and Exhibition, Houston, Texas, October 2-5.

[8] Fredd C. N., Tjia, R. and Fogler, H.S. 1997. "The Existence of an Optimum Damköhler Number for Matrix Stimulation of Carbonate Formations," SPE 38167 paper presented at the European Formation Damage Conference, The Hague, The Netherlands, 2-3 June.

[9] Fredd C. N., and Fogler, H.S. 1998a. "Alternative Stimulation Fluids and Their Impact on Carbonate Acidizing," *SPE Journal*, March, pp. 34-41.

[10] Fredd C. N., and Fogler, H.S. 1998b. "The Influence of Chelating Agents on the Kinetics of Calcite Dissolution," *Journal of Colloid Interface Science.* **204**(1): 187-197.

[11] Fredd, C.N. and Miller, M.J. 2000. "Validation of Carbonate Matrix Stimulation Models," SPE 58713 paper presented at the 2000 SPE International Symposium on Formation Damage Control, Lafayette, Louisiana, 23-24 February.

[12] Freedman, R. 2006. "Advances in NMR Logging. Journal of Petroleum Technology," paper SPE 89177, *JPT* (January 2006) 60-66.

[13] Freeman, J.J., Appel, M., Perkiins, R.B., *et al.* "Restricted Diffusion and Internal Field Gradient," SPWLA, 1999, FF.

[14] Frenier, W.W., Fredd, C.N. and Chang, F. 2001. "Hydroxyaminocarboxylic Acids Produce Superior Formulations for Matrix Stimulation for Carbonate at High Temperatures," SPE 71696 paper presented at the Annual Technical Conference and Exhibition, New Orleans, Louisiana, 30 September-3 October.

[15] Frenier, W.W., Rainey, M., Wilson, D., Crump, D. and Jones, L. 2003. "A Biodegradable Chelating Agent is Developed for Stimulation of Oil and Gas Formations," SPE 80597 paper presented at the SPE/EPA/DOE Exploration and Production Environmental Conference, San Antonio, Texas, USA, 10-12 March.

[16] Grunewald, E. and Knight, R.: "The effect of pore size and magnetic susceptibility on the surface NMR relaxation parameters T2*," Near Surf. Geophys., 9, 2011, pp.169-178.

[17] Hoefner, M.L., Fogler, H.S., Stenius, P., and Sjöblom, J. 1987. "Role of Acid Diffusion in Matrix Acidizing of Carbonates," *Journal of Petroleum Technology*, February: 203-208.

[18] Hoefner, M.L. and Fogler, H.S. 1985 "Effective Matrix Acidizing in Carbonates Using Microemulsions." *Chem. Eng. Prog.* April, 81:5

[19] Huang T., McElfresh, P.M., and Gabrysch, A.D. 2003. "Carbonate Matrix Acidizing Fluids at High Temperatures: Acetic Acid, Chelating Agents or Long-Chained Carboxylic Acids?" SPE 82268 paper presented at the European Formation Damage Conference, The Hague, The Netherlands, 13-14 May.

[20] Izgec, O., Keys, O., Zhu, D., *et al.* 2008. "An Integrated Theoretical and Experimental Study on the Effects of Multiscale Heterogeneities in Matrix

Acidizing of Carbonates," SPE 115143 paper presented at the SPE Annual Technical Conference and Exhibition, Denver, Colorado, USA, 21-24 September.

[21] Izgec, O., Zhu, D., and Hill, A.D., 2009. "Models and Methods for Understanding of Early Acid Breakthrough Observed in Acid Core-Floods of Vuggy Carbonates," SPE 122357 paper presented in the SPE European Formation Damage Conference, Scheveningen, The Netherlands, 27-29 May.

[22] Kalfayan, L., Production Enhancement with Acid Stimulation. Tulsa, OK: PennWell Books, 2008, 2nd Edition, Pages 3-5.

[23] Kleinberg, R.L., Kenyon, W.E., and Mitra, P.P. "Mechanism of NMR Relaxation of Fluids in Rock," *J. of Magn.Reson.Ser.A*, 108, 1994, pp.206-214.

[24] Korringa, J., Seevers, D.O., and Torrey, H.C. "Theory of Spin Pumping and Relaxation in Systems with a Low Concentration of Electron Spin Resonance Centers," *Phys. Rev.* 127(4), 1962, pp.1143-1150.

[25] Kubica, P. 1995. "Statistical Tests of Permeability Estimates Based on NMR Measurements," SPWLA paper presented at the 36th Annual Logging Symposium, June 26-29.

[26] LePage, J.N., De Wolf, C.A., Bemelaar, J.H., and Nasr-El-Din, H.A. 2009. "An Environmentally Friendly Stimulation Fluid for High Temperature Applications," SPE 121709 paper presented at the SPE International Symposium on Oilfield Chemistry, The Woodlands, Texas, USA, 20-22 April.

[27] Li, L, Nasr-El-Din, H.A., Chang, F.F., and Lindvig, T., 2008. "Reaction of Simple Organic Acids and Chelating Agents with Calcite," IPTC 12886 paper presented at the International Petroleum Technology Conference in Kuala Lumpur, Malaysia, 3-5 December.

[28] Mahmoud, M.A., Mohamed, I.M., Nasr-El-Din, H.A., and De Wolf, C.A. 2011. "When Should We Use Chelating Agents in Carbonate Stimulation?" SPE paper 149127 presented at the SPE/DGS Saudi Arabia Section Technical Symposium and Exhibition, al-Khobar, Saudi Arabia, 15-18 May

[29] Navarrete, R.C., Holms, B.A., McConnell, S.B., and Linton, D.E. 1998. "Emulsified Acid Enhances Well Production in High-Temperature Carbonate Formations," SPE 50612 paper presented at the SPE European Petroleum Conference, The Hague, The Netherlands, 20-22 October.

[30] Ohen, H.A., Ajufo, A.O., and Enwere, P.M. 1996. "Laboratory NMR Relaxation Measurements for the Acquisition of Calibration Data for NMR Logging Tools," SPE 35683 paper presented at the Western Regional meeting, Anchorage, Alaska, 22-24 May.

[31] Petrov, O.V., Ersland, G. and Balcom, B. 2011. "T_2 Distribution Mapping Profiles with Phase-Encode MRI," *J. of Magn. Reson.* 209: 39-46. http://dx.doi.org/10.1016/j.jmr.2010.12.006.

[32] Ramakrishnan, T.S., Schwartz, L.M., Fordhan, E.J., Kenyon, E.J., and Wilkinson, D.J.: "Forward Models for Nuclear Magnetic Resonance in Carbonate Rocks," SPWLA, 1998, SS.

[33] Reyes, E. A., Smith, A., and Beuterbaugh, A. 2013. "Carbonate Stimulation with Biodegradable Chelating Agent Having Broad Unique Spectrum (pH, Temperature, Concentration) Activity," SPE 164380 paper presented at the SPE Middle East Oil and Gas Show and Conference, Manama, Bahrain, 10-13 March.

[34] Saraf, D.N. and Fatt, I. "Three-Phase Relative Permeability Measurement Using Nuclear Magnetic Resonance for Estimating Fluid Saturation," SPE 1760, *SPE Journal*, **7**(3), September 1967, pp. 235-242.

[35] Sayed, M.A. and Nasr-El-Din. 2013 "Acid Treatments in High Temperature Dolomitic Carbonate Reservoirs Using Emulsified Acid: A Coreflooding Study," SPE 164487 paper presented at the SPE Production and Operations Symposium, Oklahoma City, Oklahoma, 23-26 March.

[36] Sayed, M.A., Nasr-El-Din, H.A., Zhou, J., Holt, S., and Al-Malki, H. 2012. "New Emulsified Acid to Stimulate Deep Wells in Carbonate Reservoirs," SPE 151061 paper presented in the SPE International Symposium and Exhibition, Lafayette, Louisiana, USA, 15-17 February.

[37] Siddiqui, S. and Khamees, A.A. 2004. "Dual-Energy CT-Scanning Application in Rock Characterization," SPE 90520 paper presented at the SPE Annual Technical Conference and Exhibition, Houston, Texas, USA, 26-29 September.

[38] Straley, C., Rossini, D., Vinegar, H., *et al.* "Core Analysis By Low-Field NMR," *The Log Analyst*, 38(2), 1997, pp. 84-95.

[39] Sørland, G.H., Djurhuus, K., Widerøe, H.C., *et al.* "Absolute Pore Size Distributions from NMR," Diffusion Fundamentals, 5, 2007, pp.4.1-1.15.

[40] Toumelin, E., Torres-Verdin, C., Chen, S., *et al*. "Analysis of NMR Diffusion Coupling Effects in Two-Phase Carbonate Rocks: Comparison of Measurements with Monte Carlo Simulations," SPWLA, 2002, JJJ.

[41] Toumelin, E., Torres-Verdin, C., Chen, S., *et al.* "Reconciling NMR Measurements and Numerical Simulations: Assessment of Temperature and Diffusive Coupling Effects on Two-Phase Carbonate Samples. Petrophysics, 44(2), 2003, pp.91-107.

[42] Valsecchi, P., McDuff, D., Chang, D., *et al.* 2012. "Simulation and Visualization of Near-Well Flow," SPE 157028 paper presented at the SPE International Production and Operation Conference and Exhibition, Doha, Qatar, 14-16 May

[43] Ziauddin, M. and Bize, E., 2007. "The Effect of Pore-Scale Heterogeneities on Carbonate Stimulation Treatments," SPE 104627 paper presented at the 15th SPE Middle East Oil & Gas Show and Conference, Bahrain, 11-14 March.

Vitae

Name :Yaser Khaled Al-Duailej

Nationality :Saudi

Date of Birth :4/28/1985

Email :yaserkd@gmail.com

Address :Dammam, Saudi Arabia

Academic Background :B.Sc. in Chemistry, 2008, King Fahd University of Petroleum and Minerals

Work Experience :Petroleum Scientist – EXPEC Advanced Research Center Saudi Aramco, Saudi Arabia (2008-Present)

Publications :- Al-Duailej, Y., Al-Khaldi, M, Hyung, K., Al-Yami, I. and Caliskan, S. 2013. "Wormholing and Deep Penetrating Acids". ADIPEC2013–679 paper presented in Abu Dhabi International Petroleum Exhibition & Conference, Abu Dhabi, UAE, 10-13 November.

- Al-Duailej, Y.K., Al-Khaldi, M.H., and Al-Kulaibi, S.A. 2012. "Triazine-Based Scavengers: Can They Be a Potential for Formation Damage?" SPE 157109 paper presented in the International Production and Operations Conference & Exhibition, Doha, Qatar, 14-16 May.
- Al-Duailej, Y.K., Al-Khaldi, M.H. and Al-Yami, I.S. 2011. "Fluids Re-Injection (FRI): A Waste Management Technique". SPE 145915 paper presented in Asia

Pacific Oil and Gas Conference and Exhibition, Jakarta, Indonesia, 20-22 September.

- Al-Duailej, Y.K., Al-Mutairi, S.H. and Al-Humaidan, A.Y. 2010. “Evaluation of Triazine-Based H_2S Scavengers for Stimulation Treatments”. SPE 136915 paper presented in Saudi Arabia Section Technical Symposium and Exhibition, Al-Khobar, Saudi Arabia, 4-7 April.